BNL-101073-2013-IR

# *A Heavy Ion Fireball freeze-out Dipion Cocktail vs Angular Correlations for Au-Au Collisions at root s=200 GeV (Part 2).*

**R. S. Longacre[1]**

[1]Brookhaven National Laboratory, Upton, NY 11973 USA

June 2013

**Physics Department**

**Brookhaven National Laboratory**

**U.S. Department of Energy**
**DOE Office of Science**

Notice: This manuscript has been co-authored by employees of Brookhaven Science Associates, LLC under Contract No. DE-AC02-98CH10886 with the U.S. Department of Energy. The publisher by accepting the manuscript for publication acknowledges that the United States Government retains a non-exclusive, paid-up, irrevocable, world-wide license to publish or reproduce the published form of this manuscript, or allow others to do so, for United States Government purposes.

This preprint is intended for publication in a journal or proceedings. Since changes may be made before publication, it may not be cited or reproduced without the author's permission.

# DISCLAIMER

This report was prepared as an account of work sponsored by an agency of the United States Government. Neither the United States Government nor any agency thereof, nor any of their employees, nor any of their contractors, subcontractors, or their employees, makes any warranty, express or implied, or assumes any legal liability or responsibility for the accuracy, completeness, or any third party's use or the results of such use of any information, apparatus, product, or process disclosed, or represents that its use would not infringe privately owned rights. Reference herein to any specific commercial product, process, or service by trade name, trademark, manufacturer, or otherwise, does not necessarily constitute or imply its endorsement, recommendation, or favoring by the United States Government or any agency thereof or its contractors or subcontractors. The views and opinions of authors expressed herein do not necessarily state or reflect those of the United States Government or any agency thereof.

# A Heavy Ion Fireball freeze-out Dipion Cocktail vs Angular Corrlations for Au-Au Collisions at $\sqrt{s_{NN}}$=200 GeV (Part 2).

R.S. Longacre[a]

[a]Brookhaven National Laboratory, Upton, NY 11973, USA

**Abstract**

In this paper we use a Cocktail fit done in Part 1 of The Dipion Cocktail, in order to compare the dipion mass spectrum within a $p_t$ range(intermediate $p_t$) with an angular correlation measured in Au-Au collisions at $\sqrt{s_{NN}}$=200 GeV which contains the same $p_t$ range. In this part(Part 2) we show that the comparison of the angular correlations in the intermediate $p_t$ range is consistent only minijet production.

## 1 Introduction

The ultra-relativistic heavy ion collision starts out as a state of high density nuclear matter called the Quark Gluon Plasma(QGP) and expands rapidly to freeze-out. During the freeze-out phase quarks and gluons form a system of strongly interacting hadrons. These hadrons continue to expand in a thermal manner until no further scattering is possible because the system becomes to dilute. However this transition from quarks and gluons(partons) into hadrons is not a smooth affair. The expansion is very rapid and some faster or hard scattered partons fragment directly into hadron through a minijet[1] process. Thus we have thermal and minijet hadrons present in the last scattering of the hadrons. The Dipion Cocktail Part 1 considered this mixture of sources and applied it to the dipion mass spectrum of the heavy ion fireball formed in Au-Au collisions at $\sqrt{s_{NN}}$=200. Part 1 showed that both thermal or soft production of hadrons and the minijet fragmented hadrons can be described through a set of unified formal equations. Part 2(this paper) applies this formalism to a $p_t$ range of dipions for Au-Au collisions at $\sqrt{s_{NN}} = 200$ GeV and 40% to 80% centrality.

The paper is organized in the following manner:

Sec. 1 Introduction. Sec. 2 Review of the two component model which we use to fit the dipion data within a $p_t$ range. Sec. 3 shows that the higher $p_t$ range is consistent with only being minijet fragmentation. Sec. 4 presents the summary and discussion.

## 2 Two component model with Breit-Wigner parameters

In this section we will alter equation 6 of Part 1 so it can use Breit-Wigner parameters (mass, width) instead of phase shifts. We will also need to modify the re-scattering part of

the equation in order to have the correct threshold behavior we have introduced in Part 1 for the minijet partial waves. The phase shift can be written for the $\ell^{th}$ wave as

$$cot\delta_\ell = \frac{(M_\ell^2 - M_{\pi\pi}^2)}{M_\ell \Gamma_\ell}, \tag{1}$$

where $M_\ell$ is the mass of the resonance in the $\ell$wave and $\Gamma_\ell$ is its total width.

$$\Gamma_\ell = \Gamma_{0\ell} \frac{\frac{qB_\ell(q/q_s)}{M_{\pi\pi}}}{\frac{q_\ell B_\ell(q_\ell/q_s)}{M_\ell}} \tag{2}$$

with $\Gamma_{0\ell}$ the total width at resonance, $B_\ell$ is the Blatt-Weisskopf-barrier factor[2] for the $\ell$ of the resonance, $q$ is the $\pi\pi$ center mass momentum, $q_\ell$ is $q$ at resonance, $M_\ell$ is the mass of the resonance, and $q_s$ is center mass momentum related to the size(1.0 fm is used $q_s = .200$ GeV/c). The Blatt-Weisskopf-barrier factor has a threshold $q^{2\ell}$ dependence.

Using equation 1 we rewrite equation 6 of Part 1 as

$$|T_\ell|^2 = |D_\ell|^2 \frac{sin^2\delta_\ell}{PS_\ell} + \frac{|A_\ell|^2 sin^2\delta_\ell}{PS_\ell} |\alpha + PS_\ell cot\delta_\ell|^2 \tag{3}$$

The $D_\ell$ is the thermal production term and is constant except for the Boltzmann weight(see equation 13 in Part 1). The expected threshold behavior $q^{2\ell+1}$ comes from the $sin\delta_\ell$ term. Since there is $sin^2\delta_\ell$ one of the $q^{2\ell+1}$ is killed off by dividing by $PS_\ell$.

$$PS_\ell = \frac{2qB_\ell(q/q_s)}{M_{\pi\pi}} \tag{4}$$

In Figure 6 of Part 1 we have put into our minijet $A_\ell$ the correct threshold $q^{2\ell+1}$ so we need to kill off the $q^{2\ell+1}$ of the other $sin\delta_\ell$ term. Therefore the above equation for our minijet $A_\ell$ we will use

$$|T_\ell|^2 = |D_\ell|^2 \frac{sin^2\delta_\ell}{PS_\ell} + \frac{|A_\ell|^2 sin^2\delta_\ell}{PS_\ell^2} |\alpha + PS_\ell cot\delta_\ell|^2 \tag{5}$$

Rewriting equation 6 of Part 1 for each partial wave with Breit-Wigner parameters the first term becomes

$$|T_\ell|_1^2 = |D_\ell|^2 \frac{M_{\pi\pi}^2}{\sqrt{M_{\pi\pi}^2 + p_t^2}} exp \frac{-\sqrt{M_{\pi\pi}^2 + p_t^2}}{T} \frac{M_\ell \Gamma_\ell}{(M_\ell^2 - M_{\pi\pi}^2)^2 + M_\ell^2 \Gamma_\ell^2}, \tag{6}$$

while the second term

$$|T_\ell|_2^2 = |A_\ell|^2 \frac{M_\ell^2 \Gamma_\ell^2}{(M_\ell^2 - M_{\pi\pi}^2)^2 + M_\ell^2 \Gamma_\ell^2} \left| \alpha + \frac{2qB_\ell(\frac{q}{q_s})(M_\ell^2 - M_{\pi\pi}^2)}{M_{\pi\pi} M_\ell \Gamma_\ell} \right|^2 \left( \frac{M_{\pi\pi}^2}{4q^2 B_\ell^2(\frac{q}{q_s})} \right). \tag{7}$$

$$|T|^2 = \sum_\ell |T_\ell|^2 \tag{8}$$

where

$$|T_\ell|^2 = |T_\ell|_1^2 + |T_\ell|_2^2 \tag{9}$$

and $|A_0|^2 = S(M_{\pi^+\pi^-})$,$|A_1|^2 = P(M_{\pi^+\pi^-})$,$|A_2|^2 = D(M_{\pi^+\pi^-})$, and $|A_3|^2 = F(M_{\pi^+\pi^-})$. S, P, D and F comes from subsection 5.2 of Part 1.

## 2.1 STAR data dipion $p_t$ range (1.6 GeV/c $< p_t <$ 1.8 GeV/c)

We have fitted a dipion $p_t$ range using equation 8 above for the STAR data Au-Au collisions at $\sqrt{s_{NN}} = 200$ GeV 40% to 80% centrality. We included minijets up to $\ell = 3$ and resonances $\sigma$ $\ell = 0$, $\rho(770)$ $\ell = 1$, and $f_2(1270)$ $\ell = 2$. Using the arguments of Sec. 3 Part 1 we added the $f_0$ as a direct thermal term ($|T_0|_1^2$) and only the $\sigma$ interfered with $\ell = 0$ minijet background. Two other thermal terms are present in the cocktail, the $K_S^0$ and the $\omega_0$.

Finally the threshold effective mass region .280 GeV to .430 GeV is dominated by the Swave and receives contributions from minijet fragmentation, $\pi\pi$ Swave phase shift, $\eta$ decay, HBT adding to the like sign $\pi\pi$ distribution that has been subtracted away from the unlike sign $\pi\pi$ and the coulomb correction between the charged pions. The minijet fragmentation is the least known of the effects since we relied on PYTHIA[3], however there are large uncertainty in all the other effects. So for this fit we let the minijet fragmentation be free to fit the data and let the Breit-Wigner parameters for the $\sigma$ determine the Swave phase shifts plus leaving out all other effects. The results of this fit is shown in Figure 1. Table I shows the Breit-Wigner parameters used in the fit.

**Table I.** The Bret-Wigner Parameters of the fit.

| Table I | | |
|---|---|---|
| resonance | mass(GeV) | width(GeV) |
| $\sigma$ | 1.011 | 1.015 |
| $f_0$ | 0.973 | 0.041 |
| $\rho$ | 0.748 | 0.147 |
| $f_2$ | 1.275 | 0.185 |

Equation 6 has an important factor the coefficient $\alpha$. This coefficient is related to the real part of the $\pi\pi$ re-scattering loop and is given by equation 9. When the pions re-scatter or interact at a close distance or a point the real part of the loop $\alpha$ has its maximum value of $\alpha_0$. While if the pions re-scatter or interact at a distance determined by the diffractive limit the value of $\alpha$ is zero. The $\alpha$ which is the real part of the re-scattering factor has a simple form given by

$$\alpha = (1.0 - \frac{r^2}{r_0^2})\alpha_0 \tag{10}$$

where $r$ is the radius of re-scattering in fm's and $r_0$ is 1.0 fm or the limiting range of the strong interaction ranging to $r = 0.0$ for point like interactions.

The value of $\alpha_0$ used is equal to 2.0 as determined in Appendix B of Part 1. Thus the radius of the size associated with re-scattering is .773 fm for this $p_t$ range from equation 9.

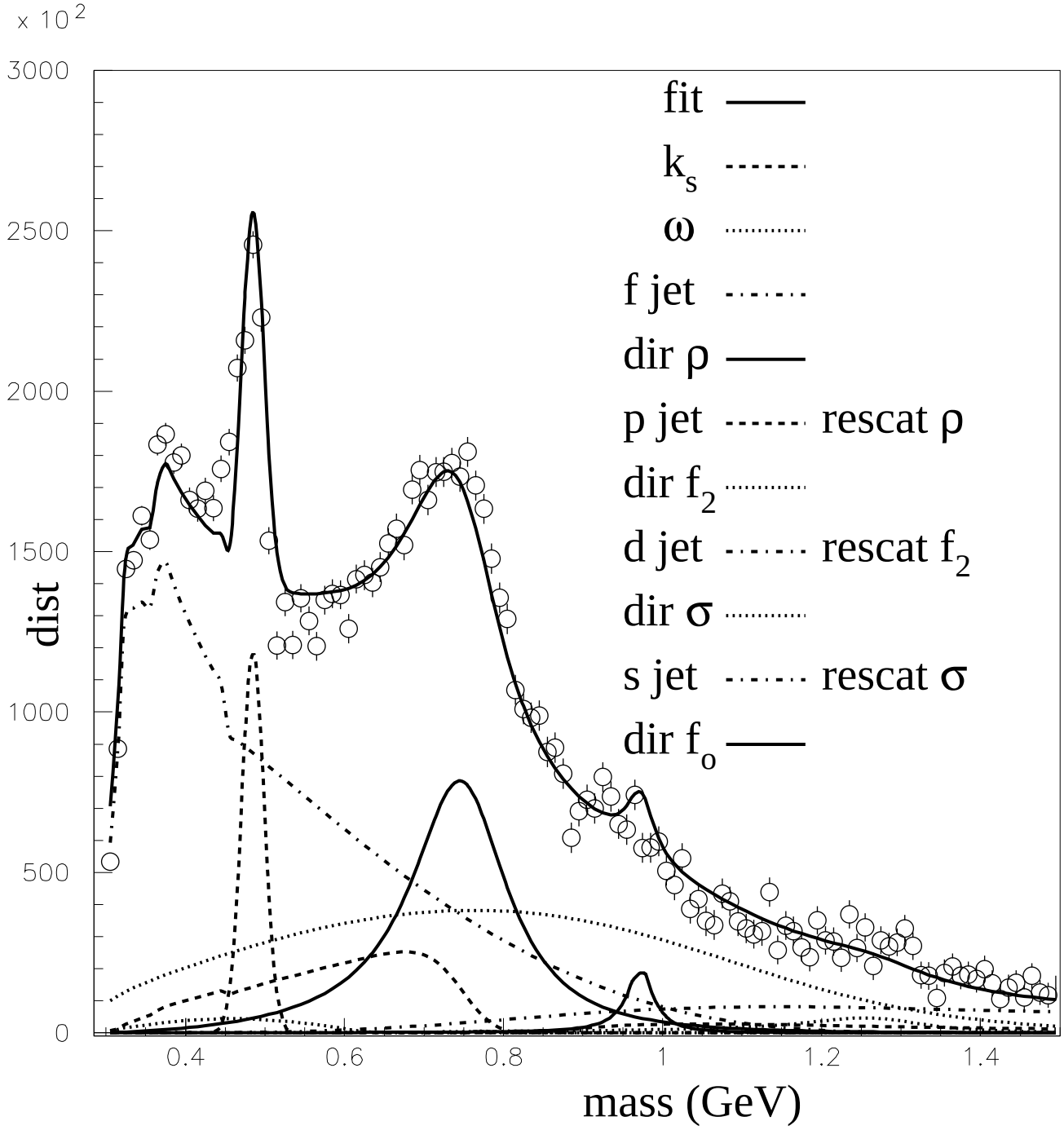


Figure 1: Fit to STAR dipion effective mass distribution (1.6 GeV/c $< p_t <$ 1.8 GeV/c) for Au-Au collisions at $\sqrt{s_{NN}} = 200$ GeV 40% to 80% centrality using equation 8. See text for complete information.

# 3 Minijet measured directly and level seen in dipion effective mass spectrum

A direct measurement of minijets is done through two particle angular correlations[4]. There are two models which can reproduce the angular correlations seen in central Au-Au collisions at $\sqrt{s_{NN}} = 200$ GeV[4]. Both models rely on parton fragmentation like that of PYTHIA[3]. The correlation can be reproduced over a wide range of $p_t$. Thus we should be able to use a $p_t$ range consistent with the dipion $p_t$ cuts used above. The downside of the above analysis is that it is done for central events and we want more peripheral events. Ref.[5, 6] has done a centrality study using one of the models (flux tube model) comparing to STAR data with a $p_t$ range (0.8 GeV/c $< p_t <$ 4.0 GeV/c) for charge particles. Using this analysis one can determine how to scale two particle angular correlation to more peripheral events. Ref.[7] uses the other model (minijet model) and STAR data as a function of centrality over a much wider range of $p_t$ ($p_t >$ 0.15 GeV/c) and finds a different scaling of the two particle angular correlations. Thus we should be able to build a simple model based on PYTHIA[3] and HIJING[8] and the above analyses to make a prediction for the minijet dipion spectrum.

## 3.1 Determining the Charge Dependent Minijet Correlation for the Dipion Comparison

We will first consider the flux tube model[4] and the centrality extrapolation that has been show to work well in reproducing the Charge Dependent Correlation function, see Refs[5, 6]. The dipion effective spectrum presented above is close to the $p_t$ range where the flux tube model works best.

The flux tubes arise from wavefunctions of the incoming projectiles of sheets of color glass condensates (CGC)[9] that at these high energies collide, interact, and evolve into high intensity color electric and magnetic fields. These primordial fields are initially composed of only rapidity independent longitudinal color electric and magnetic fields. An essential feature of the flux tube is that the fields are localized in the transverse space of the collision zone with a size of $1/Q_s$. $Q_s$ is the saturation momentum of partons in the nuclear wavefunction. These longitudinal color electric and magnetic fields generate topological Chern-Simons charge[10] which becomes a source for particle production.

The transverse space is filled with flux tubes of large longitudinal extent but small transverse size $\sim Q_s^{-1}$. Particle production from a flux tube is a Poisson process, since the flux tube is a coherent state. The flux tubes at the center of the transverse plane interact with each other through plasma instabilities[11, 12] and create a locally thermalized system, where partons emitted from these flux tubes are locally equilibrated. A hydro system with transverse flow builds causing a radially flowing blast wave[13]. The flux tubes that are near the surface of the fireball get the largest radial flow and are emitted from the surface.

This surface fragmentation is made up of a series of partons that are aligned along the radially flowing flux tube. Each partons under goes a PYTHIA like fragmentation. These

partons are mainly electric charge neutral gluons and their balancing charge is contained with in the fragmentation of an individual parton. We can form two types of angular correlation functions the Charge Independent(CI) and the Charge Dependent(CD). The CI correlation consider all charged particle independent of their charge while the CD correlation is the difference between the unlike charged pairs and the like charged pairs. The CD correlation and the balance function is very much the same measure in terms of determining the angular spread of balancing pairs. Refs.[5, 6] demonstrate that for the $p_t$ range (0.8 GeV/c $< p_t <$ 4.0 GeV/c) the surface flux tubes can be extrapolated to other centralities. The CI correlation show the largest changes in the $\Delta\eta$ width when on goes from central to peripheral see Figure 2. This change in width happens because for central events the flux tube is a chain of partons aligned at a single $\phi$ value and different $\eta$ values becoming only a single parton or minijet at very peripheral collisions. For the CD correlation the $\Delta\eta$ width is determined by a single parton fragmenting as pointed out above and therefore shows no change of $\Delta\eta$ width with centrality see Figure 3. In Figure 4 we show the signal strength of the CD correlation as a function of centrality. We see that this signal strength varies in a smooth linear way with centrality.

Ref.[4] divided central events up into 7 ranges of $p_t$ (see Table II). Since we are choosing particle pairs, we choose for the first particle $p_{t1}$ which could be in one bin and for the second particle $p_{t2}$ which could be in another bin. Therefore binning implies a matrix of $p_{t1}$ vs $p_{t2}$. We have 7 bins thus there are 28 independent combinations. The $p_t$ combinations that would have a large overlap with the dipion $p_t$ range (1.6 GeV/c $< p_t <$ 1.8 GeV/c) is P6P6 for symmetric $\pi\pi$ and P4P7 for asymmetric $\pi\pi$. Lower edge of P6P6 0.8 GeV/c times two equals 1.6 GeV/c. P4P7 lower edge 0.5 GeV/c plus 1.1 GeV/c equals 1.6 GeV/c.

**Table II.** The $p_t$ bins and the number of charged particles per bin with $|\eta| < 1.0$.

| Table II | |
|---|---|
| $p_t$ range | amount |
| $0.3GeV/c - 0.2GeV/c$ | 291 |
| $0.4GeV/c - 0.3GeV/c$ | 260 |
| $0.5GeV/c - 0.4GeV/c$ | 208 |
| $0.65GeV/c - 0.5GeV/c$ | 230 |
| $0.8GeV/c - 0.65GeV/c$ | 152 |
| $1.1GeV/c - 0.8GeV/c$ | 171 |
| $4.0GeV/c - 1.1GeV/c$ | 149 |

## 3.2 Making a simple PYTHIA model for extrapolation

We first need to create a simple model using PYTHIA and HIJING that is a good approximation to the angular correlations for central Au-Au collisions at $\sqrt{s_{NN}} = 200$ GeV. For scaling from central to peripheral we need the unlike, like, and the CD for $p_t$ bin 7 and 6 combined since this is the binning of Refs.[5, 6]. Then for comparing with the dipion $p_t$ range we need the unlike, like, and the CD for P6P6 and P4P7. For central events these correlations are shown in Figure 5 through Figure 13.

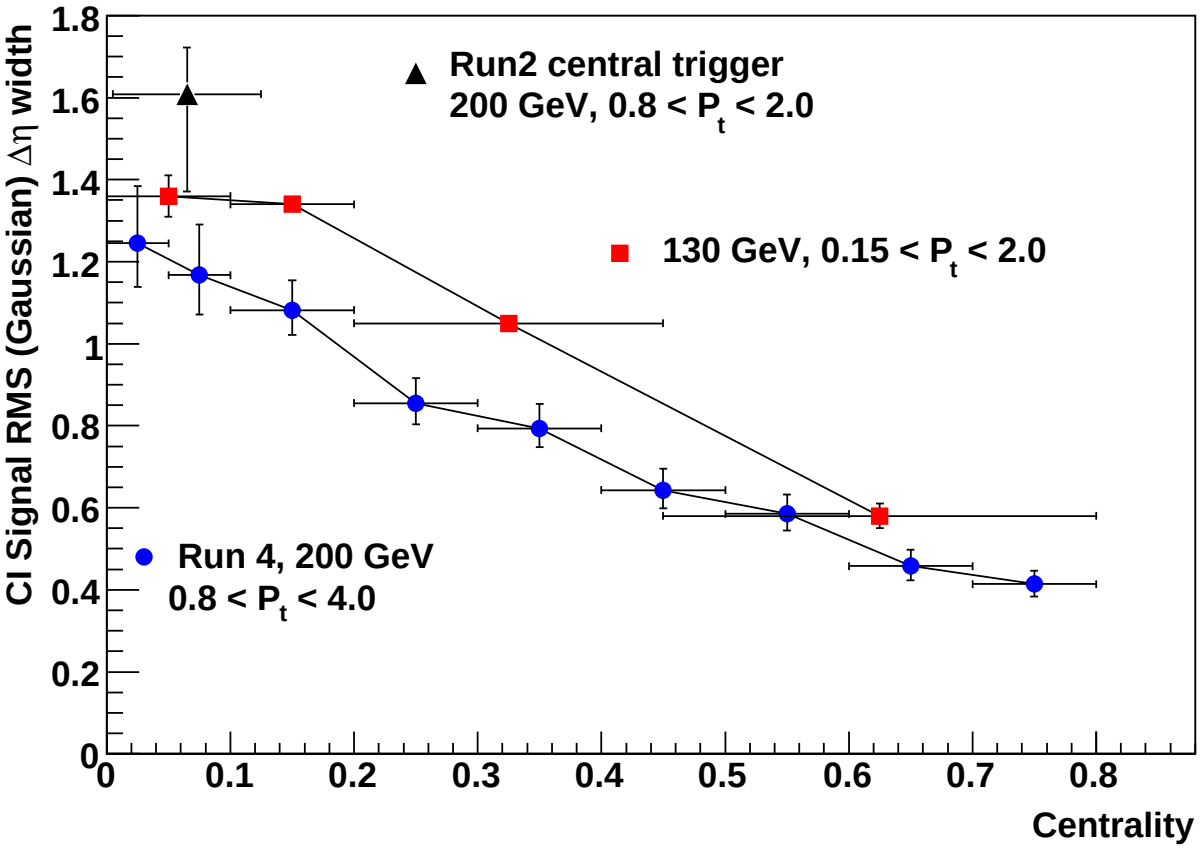


Figure 2: The CI $\Delta\eta$ width (GaussianRMS) vs. centrality for the analyses indicated. The differences between the present analysis and the 130 GeV analysis are attributed to the preponderance of low energy particles in the 130 GeV analysis. The 130 GeV analysis is similar to Ref.[7].

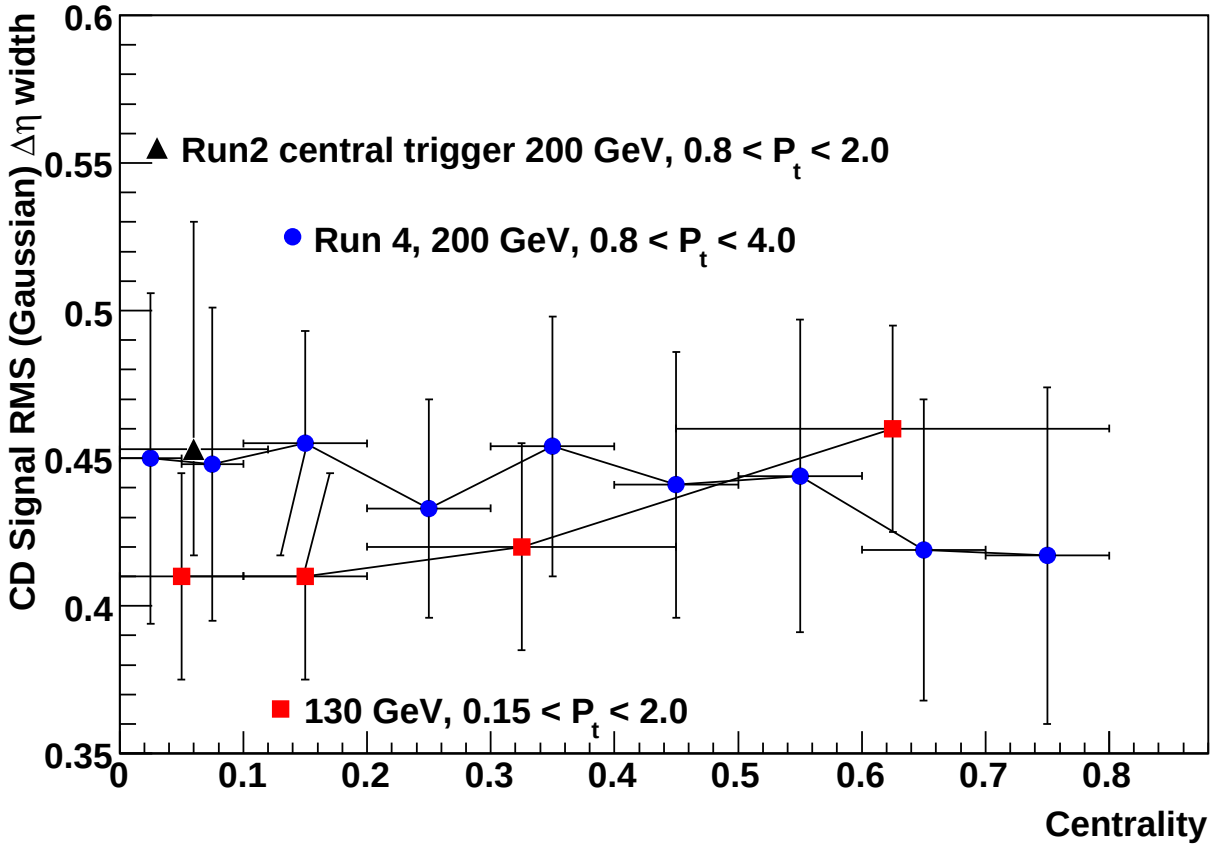


Figure 3: The CD $\Delta\eta$ width vs. centrality.

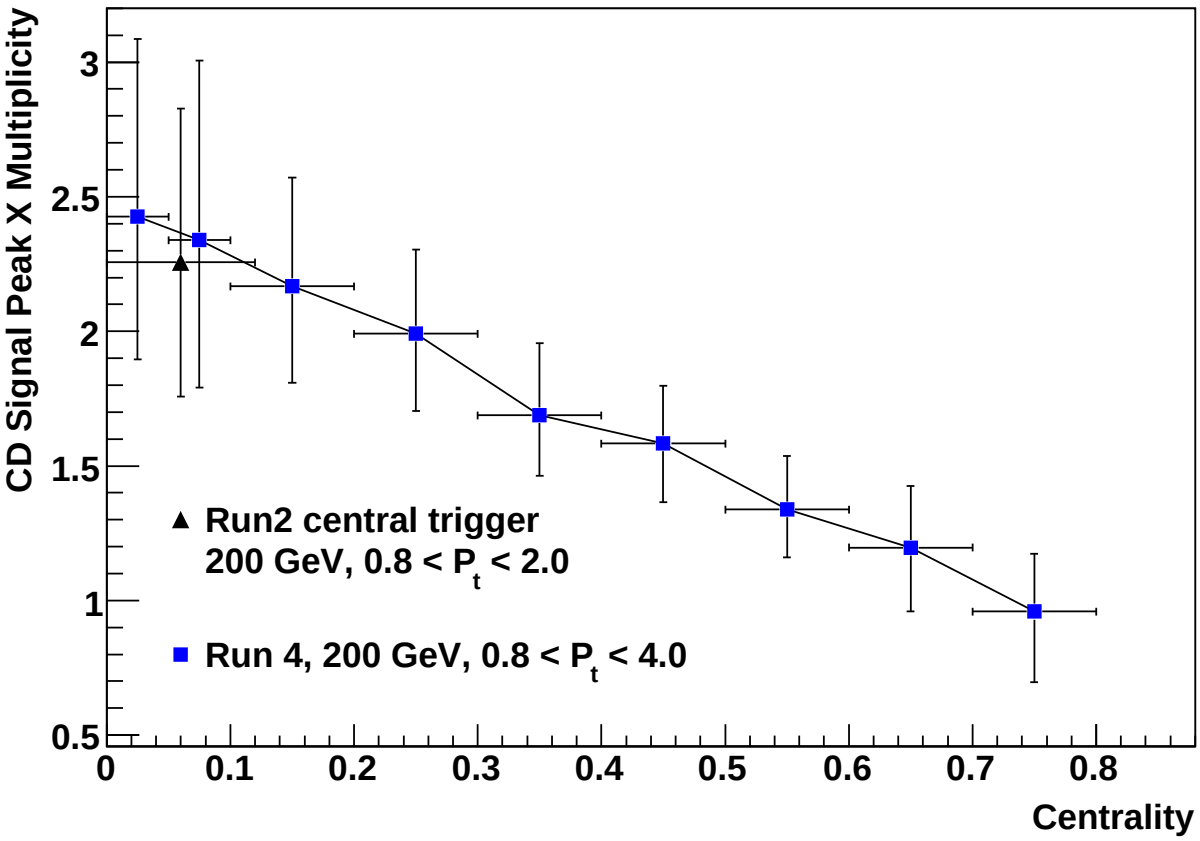


Figure 4: The CD signal strength vs. centrality.

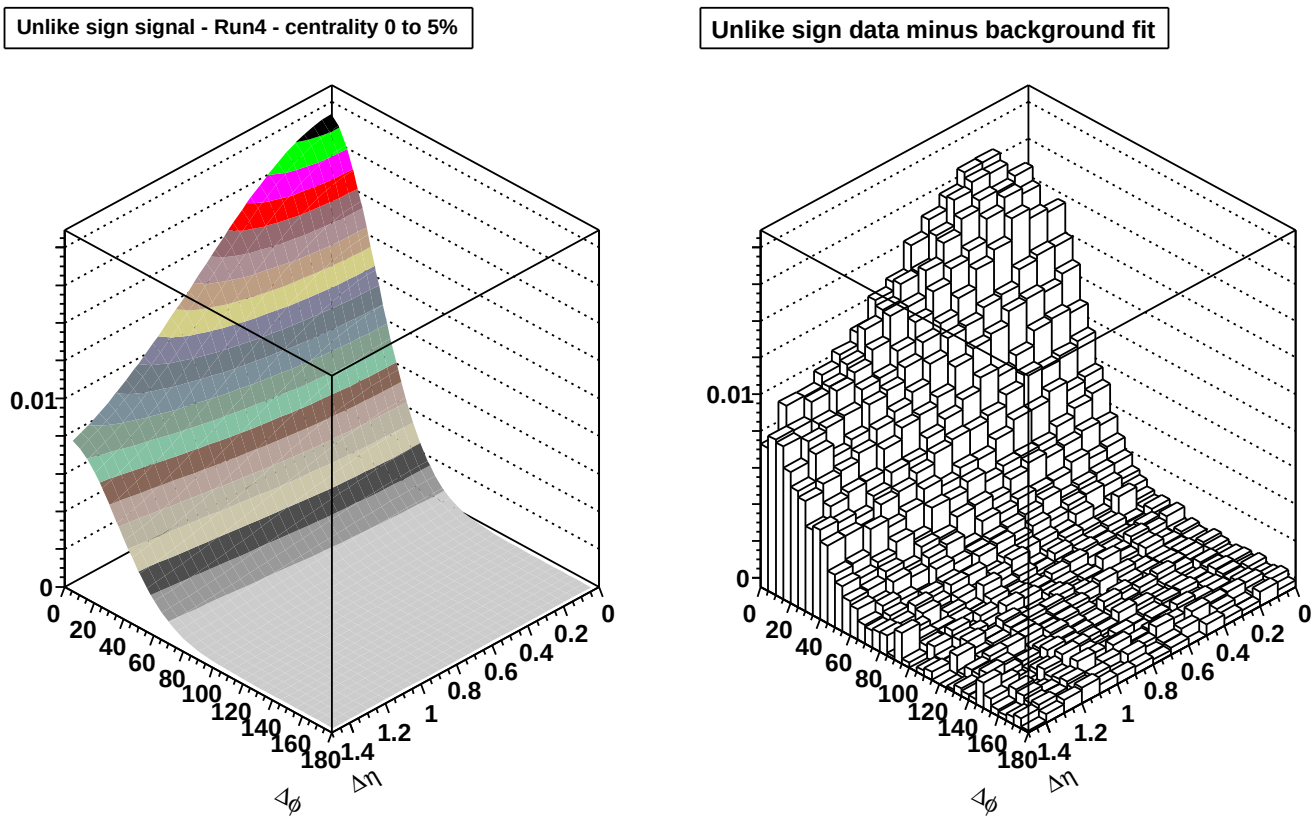


Figure 5: a) 2-D perspective plot fit to the unlike signal (equation 3 of Ref.[5]) in the 0-5% centrality bin (most central). b) The unlike signal data that were used in the fit.

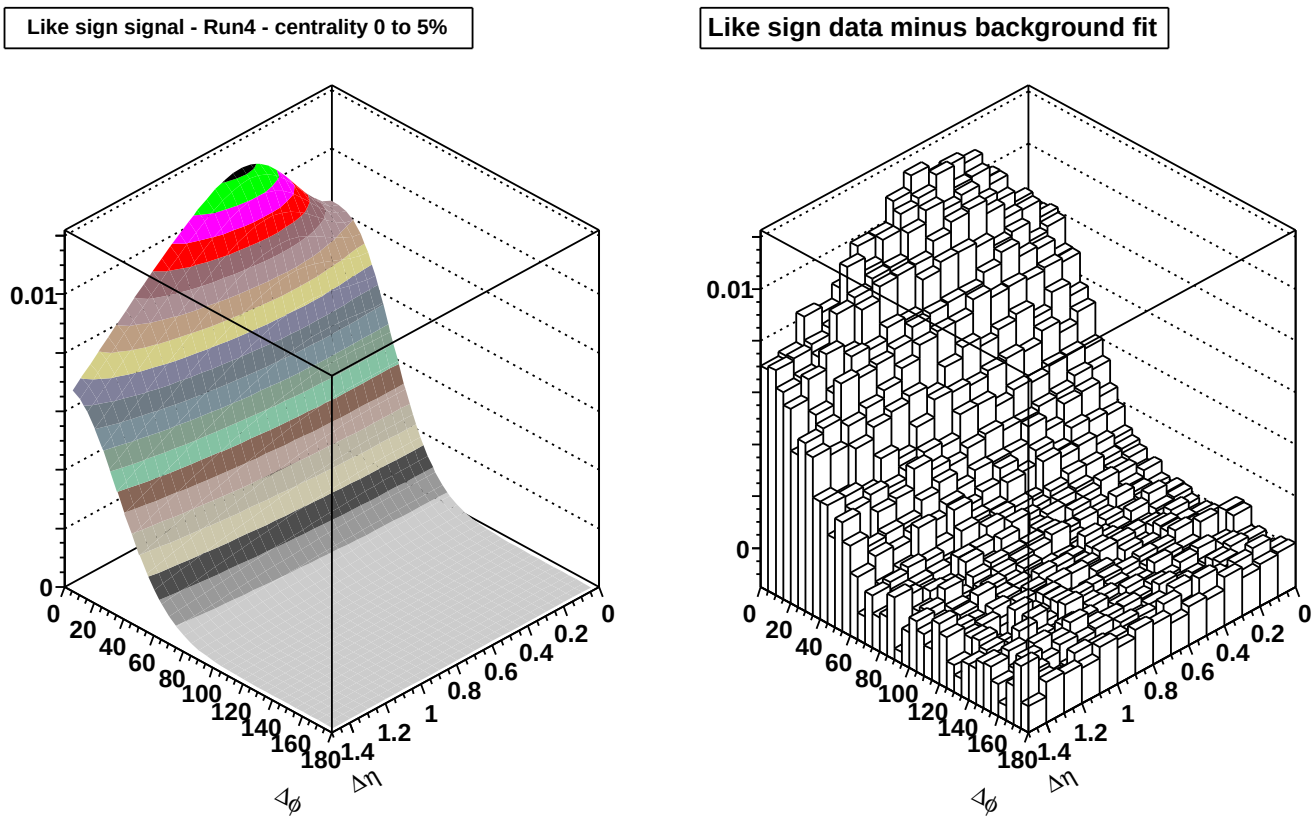


Figure 6: a) 2-D perspective plot fit to the like signal (equation 4 of Ref.[5]) in the 0-5% centrality bin (most central). b) The like signal data that were used in the fit.

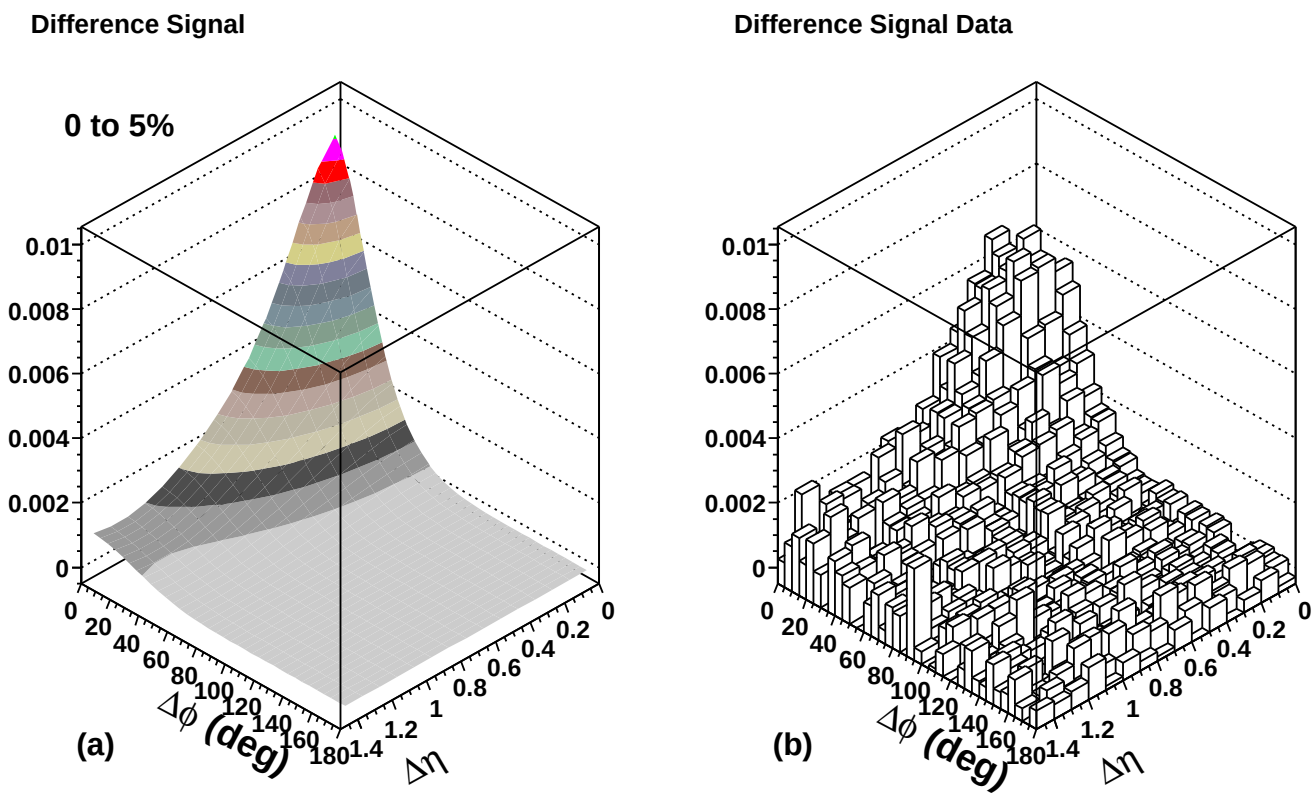


Figure 7: a) 2-D perspective plot difference between the unlike signal and the the like signal (equation 3 - equation 4 of Ref.[5]) in the 0-5% centrality bin (most central). b) The CD signal data that were used in the fit.

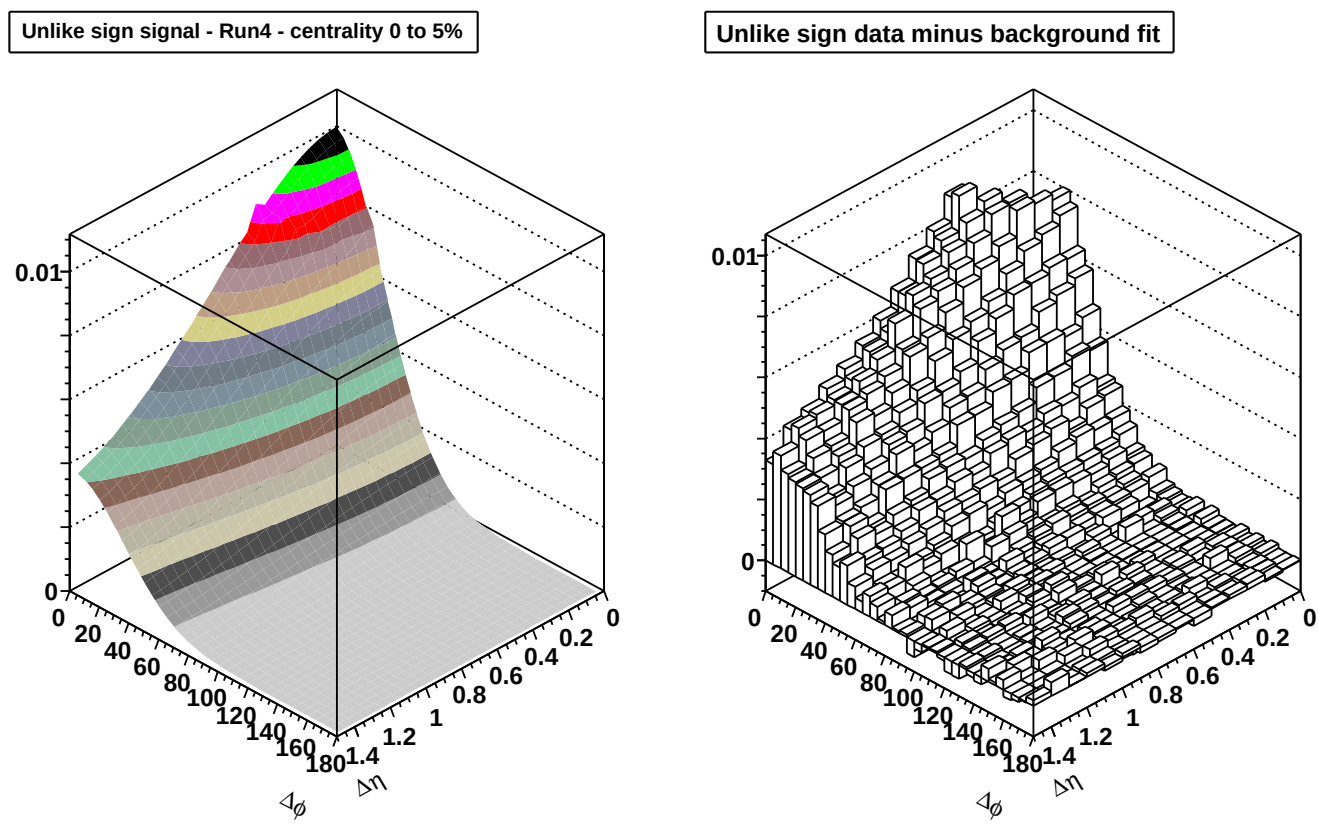


Figure 8: a) 2-D perspective plot fit to the unlike signal for P6P6 $p_t$ cuts(see text) in the 0-5% centrality bin (most central). b) The unlike signal data that were used in the fit.

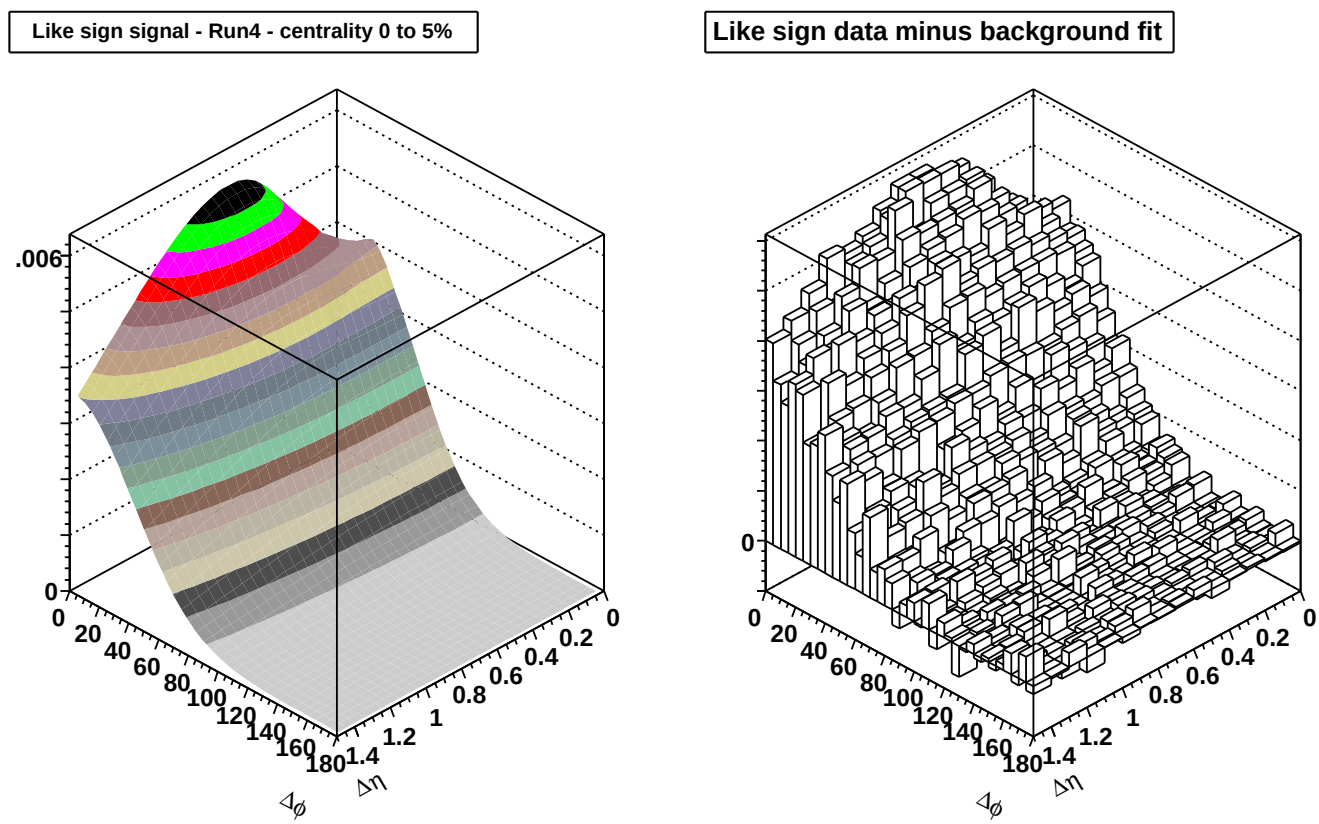


Figure 9: a) 2-D perspective plot fit to the like signal for P6P6 $p_t$ cuts(see text) in the 0-5% centrality bin (most central). b) The like signal data that were used in the fit.

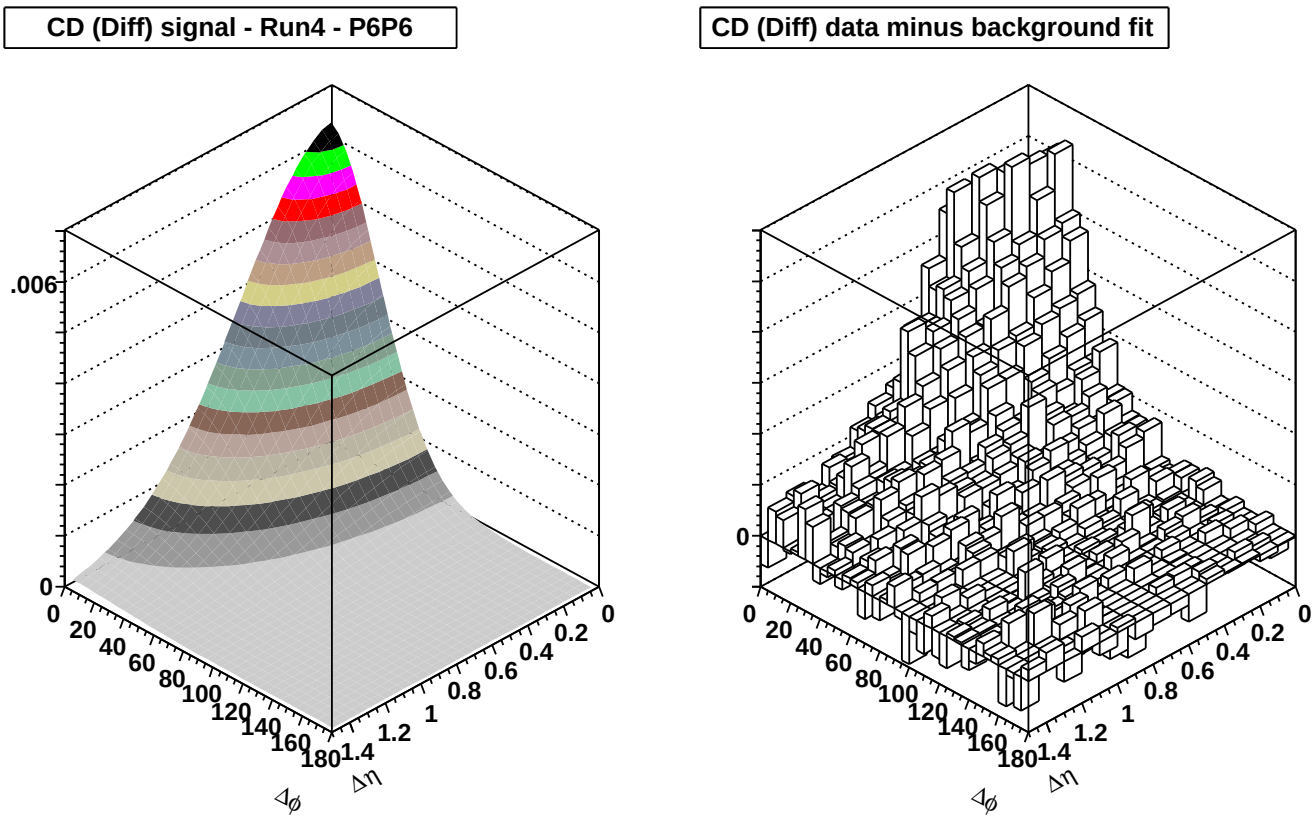


Figure 10: a) 2-D perspective plot difference between the unlike signal and the the like signal P6P6(Figure 8 - Figure 9) in the 0-5% centrality bin (most central). b) The CD signal data that were used in the fit.

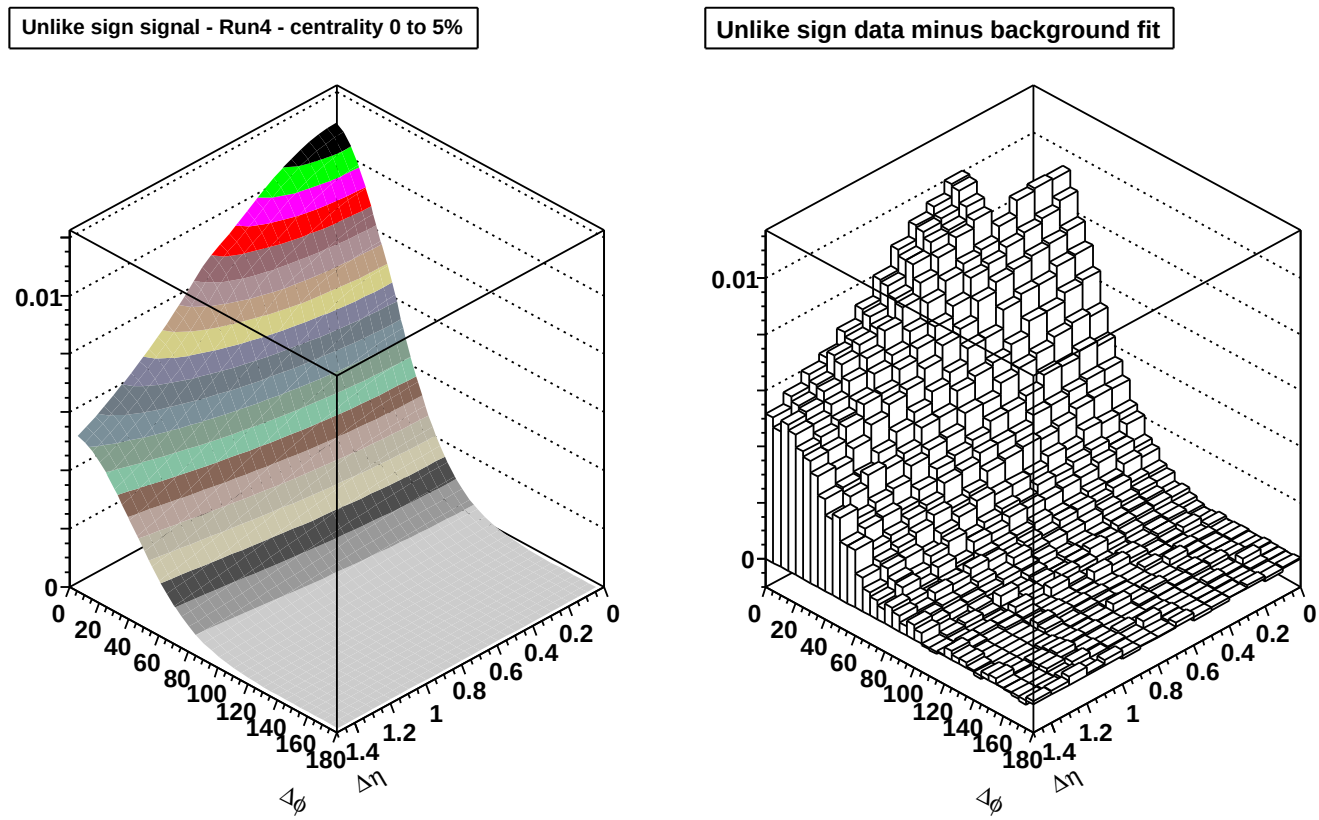


Figure 11: a) 2-D perspective plot fit to the unlike signal for P4P7 $p_t$ cuts(see text) in the 0-5% centrality bin (most central). b) The unlike signal data that were used in the fit.

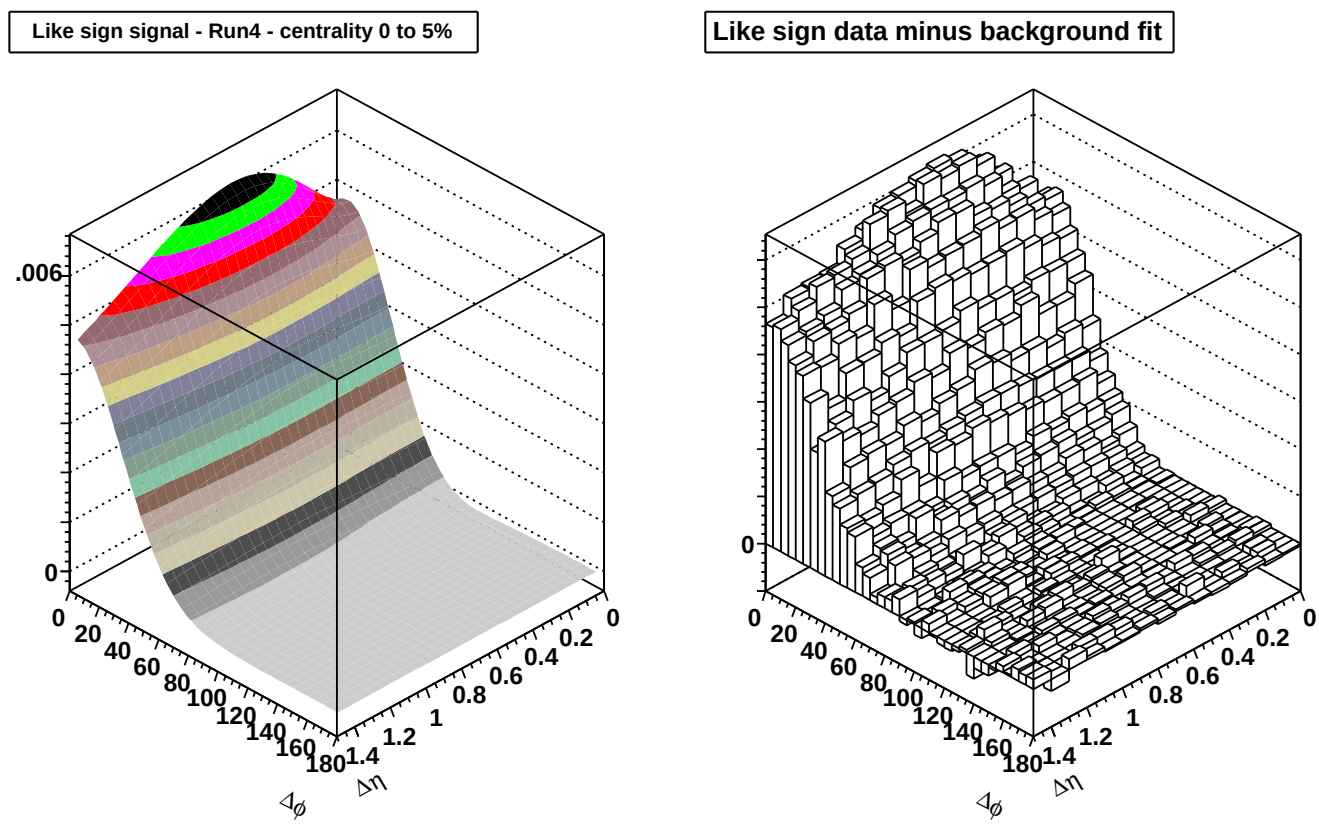


Figure 12: a) 2-D perspective plot fit to the like signal for P4P7 $p_t$ cuts(see text) in the 0-5% centrality bin (most central). b) The like signal data that were used in the fit.

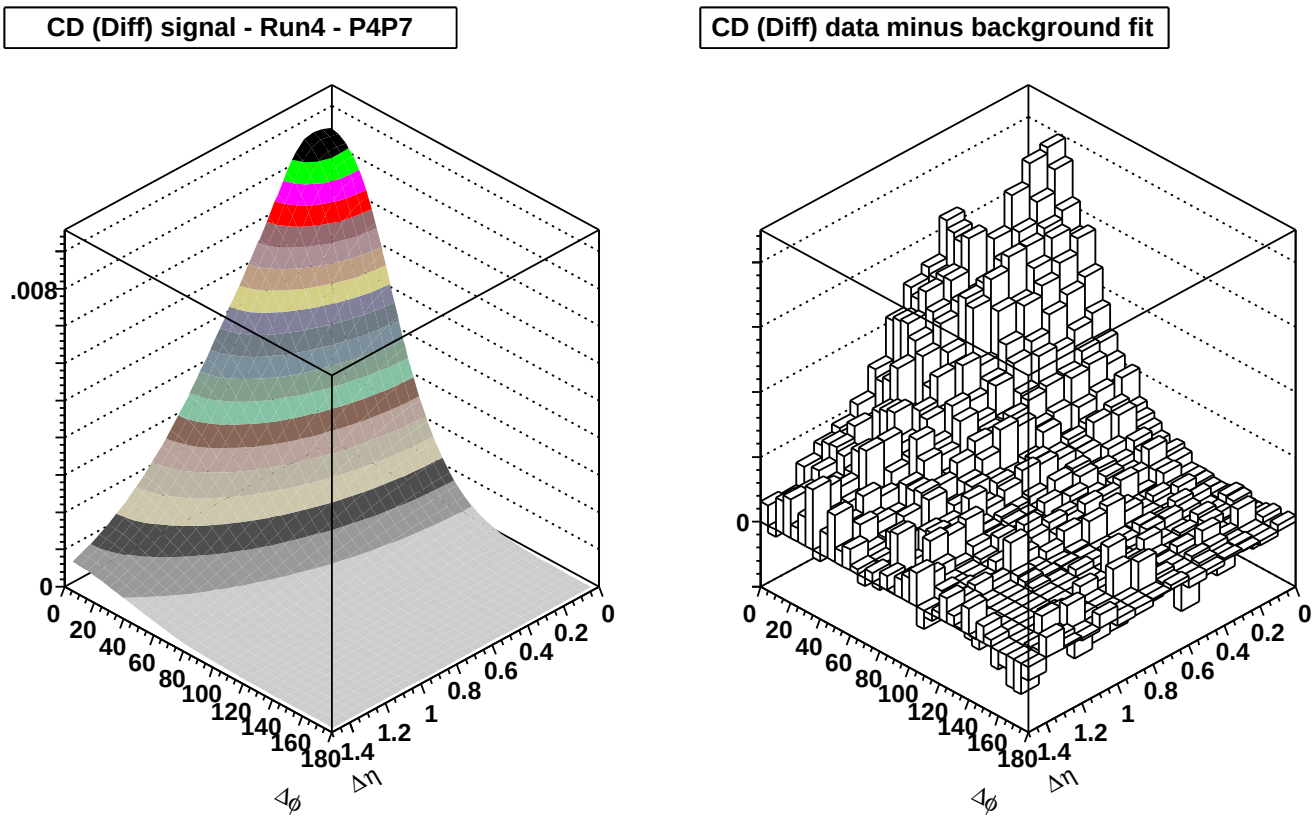


Figure 13: a) 2-D perspective plot difference between the unlike signal and the the like signal P4P7(Figure 11 - Figure 12) in the 0-5% centrality bin (most central). b) The CD signal data that were used in the fit.

Note that for the like sign pairs there is a dip near $\Delta\phi$ and $\Delta\eta$ equals zero. In Ref.[14] it was shown that the dip or depletion of same charge particles is due to presence of the strong longitudinal color electric fields of the flux tubes. Quarks and anti-quarks are created in pairs of color and anti-color and feel the strong color electric field and are pushed part. Each color pair are pushed in the same direction. This pushing and alignment keeps unlike charges close together and separates like charges.

We make a simple minijet model using PYTHIA to fragment the partons and HIJING to complete the particle number without adding any additional correlations. Each event has the same parton $p_t$ distribution that was used in the flux tubes[4]. We did not align the partons along a flux tube because it plays no role in the CD correlation. The dipion effective mass spectrum like the CD correlation and the balance function is the difference between unlike charge pairs and like charge pairs. We adjust the HIJING particles and the PYTHIA fragmented partons in order to reproduce the core unlike and like correlations plus obtaining a very good CD correlation for the central data Figure 8 through Figure 13. It turns out that in our simple model the CD correlation for P6P6 is very close to P4P7 and has a peak value of 0.007.

Figure 14 through Figure 16 is the 50% to 60% centrality for $p_t$ range (0.8 GeV/c $< p_t <$ 4.0 GeV/c) which is the range that we have shown has a good extrapolation for the surface emitted partons of the flux tube. We keep our model the same and only reduce the particle number from HIJING and the fragmenting parton number from PYTHIA until we reproduce very completely the unlike, like and CD correlations of Figure 14 through Figure 16. The spread in $\Delta\eta$ is not very important at this centrality. Using this extrapolation we can predict the yield for P6P6 and P4P7 for the unlike and like correlations which we show in Figure 17 through Figure 20.

With the extrapolation model of the surface flux tube model we are able to generate Au-Au events for centrality 50% to 60%. We compare this dipion effective mass spectrum generated by PYTHIA fragmentation from partons that fragment near the surface of the fireball. This comparison is shown in Figure 26 to the STAR data for dipion $p_t$ (1.6 GeV/c $< p_t <$ 1.8 GeV/c).

The flux tube model assumes that these are the only partons present. Ref.[5] show that for STAR data choosing a $p_t$ range (0.8 GeV/c $< p_t <$ 4.0 GeV/c) that only these surface flux tubes are important. For central collisions flux tubes that are inside the volume of the fireball interact with each other through plasma instabilities[11, 12] and create a locally thermalized system, where partons emitted from these flux tubes are locally equilibrated. A hydro system with transverse flow builds causing a radially flowing blast wave[13]. The flux tubes that are near the surface of the fireball get the largest radial flow and are emitted from the surface. This surface flow and emission also happens at the middle centrality range except the center of the fireball may not be so completely thermalized and partons from the center should also fragment and escape.

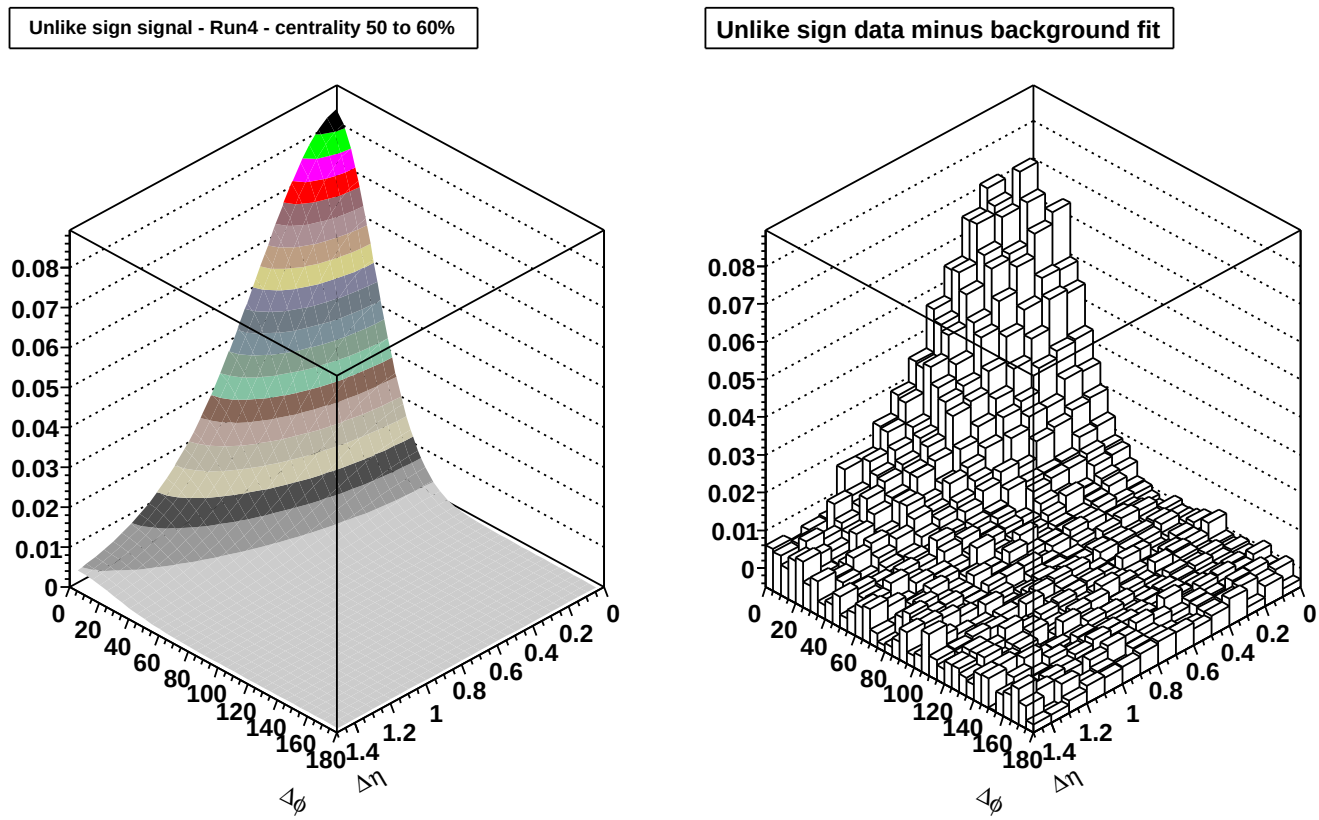


Figure 14: a) 2-D perspective plot fit to the unlike signal (equation 3 of Ref.[5]) in the 50%-60% centrality bin. b) The unlike signal data that were used in the fit.

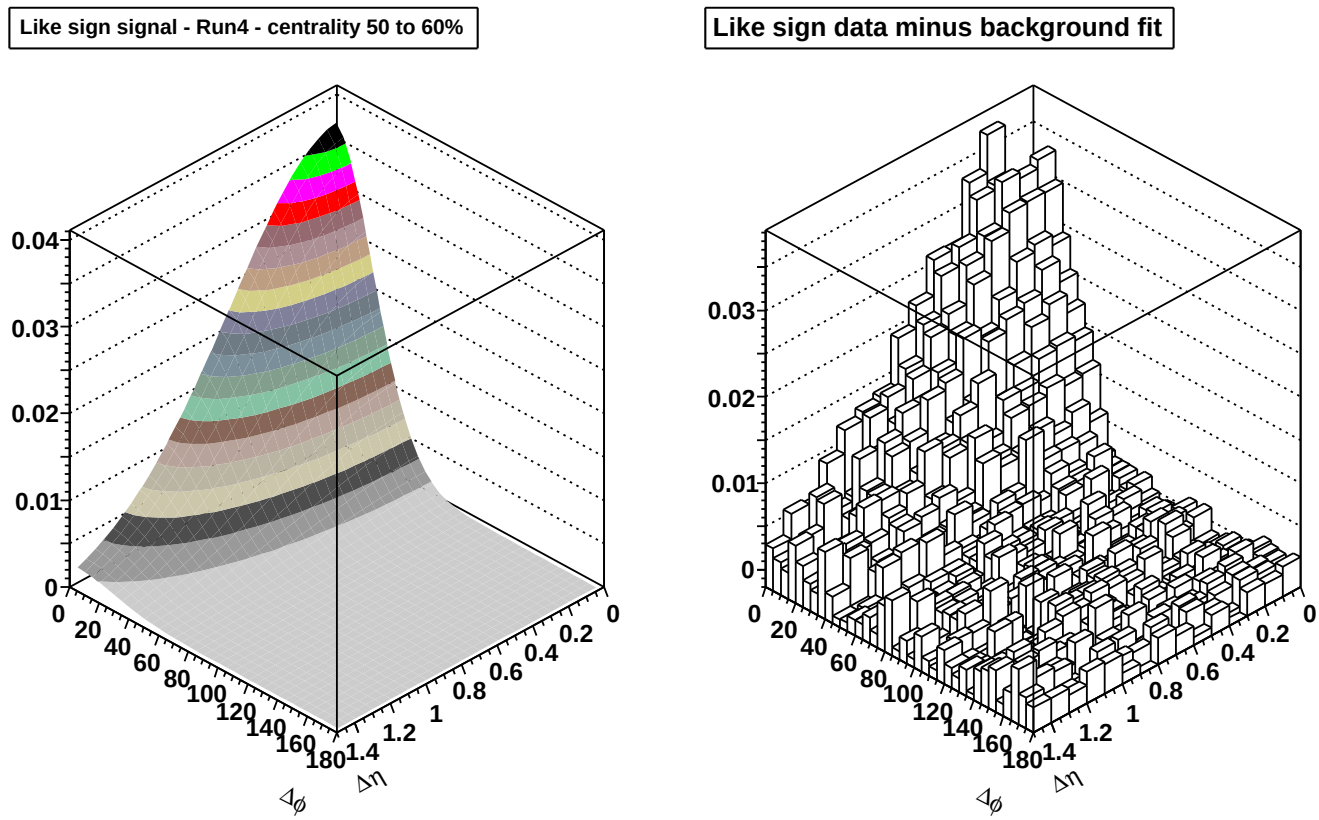


Figure 15: a) 2-D perspective plot fit to the like signal (equation 4 of Ref.[5]) in the 50%-60% centrality bin. b) The like signal data that were used in the fit.

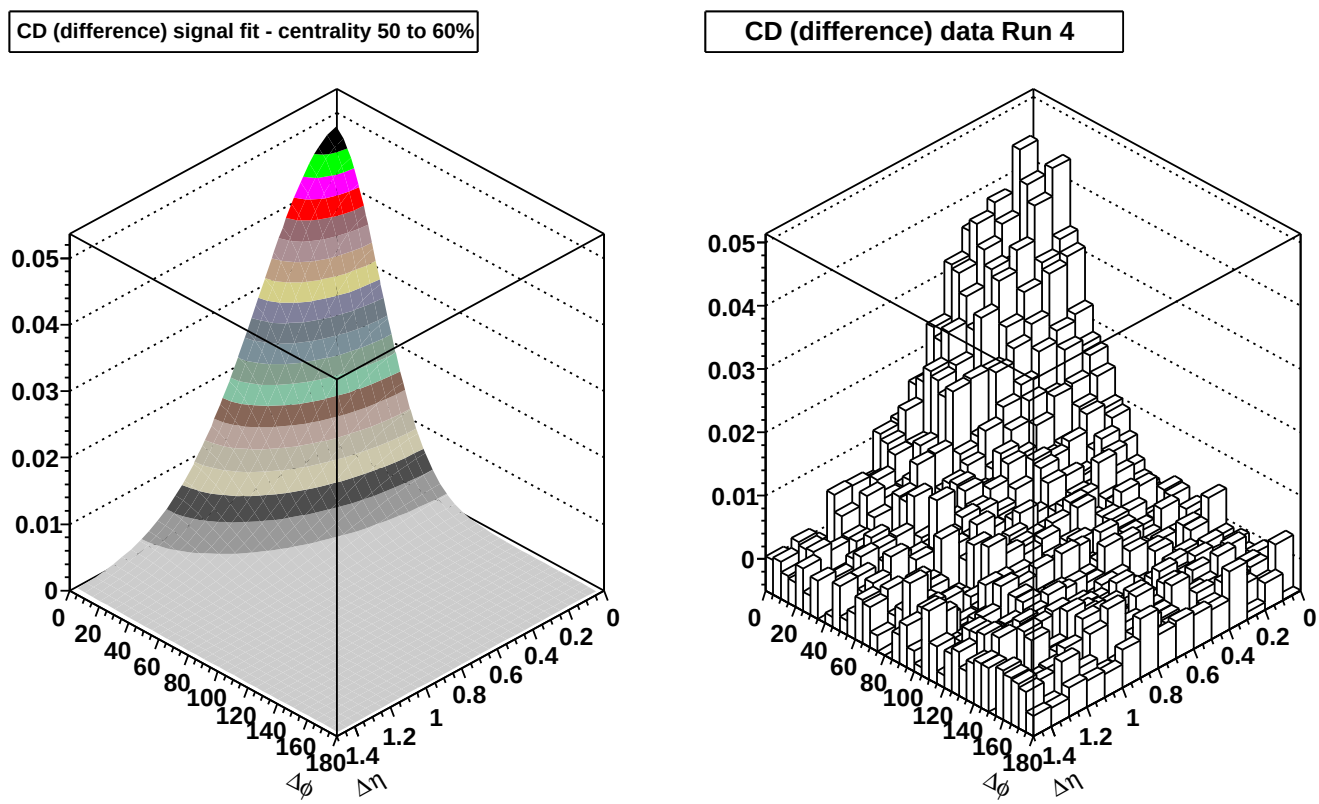


Figure 16: a) 2-D perspective plot difference between the unlike signal and the the like signal (equation 3 - equation 4 of Ref.[5]) in the 50%-60% centrality bin. b) The CD signal data that were used in the fit.

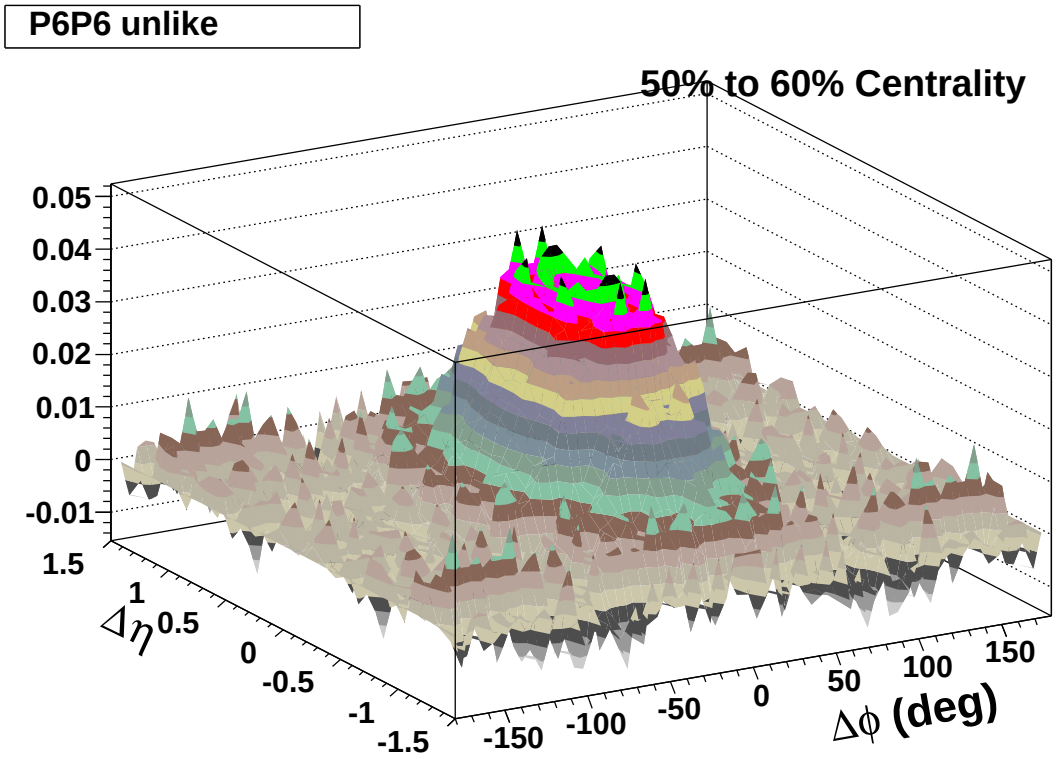


Figure 17: 2-D perspective plot using our extrapolation model(see text) of the unlike signal for P6P6 $p_t$ cuts(also see text) in the 50%-60% centrality bin.

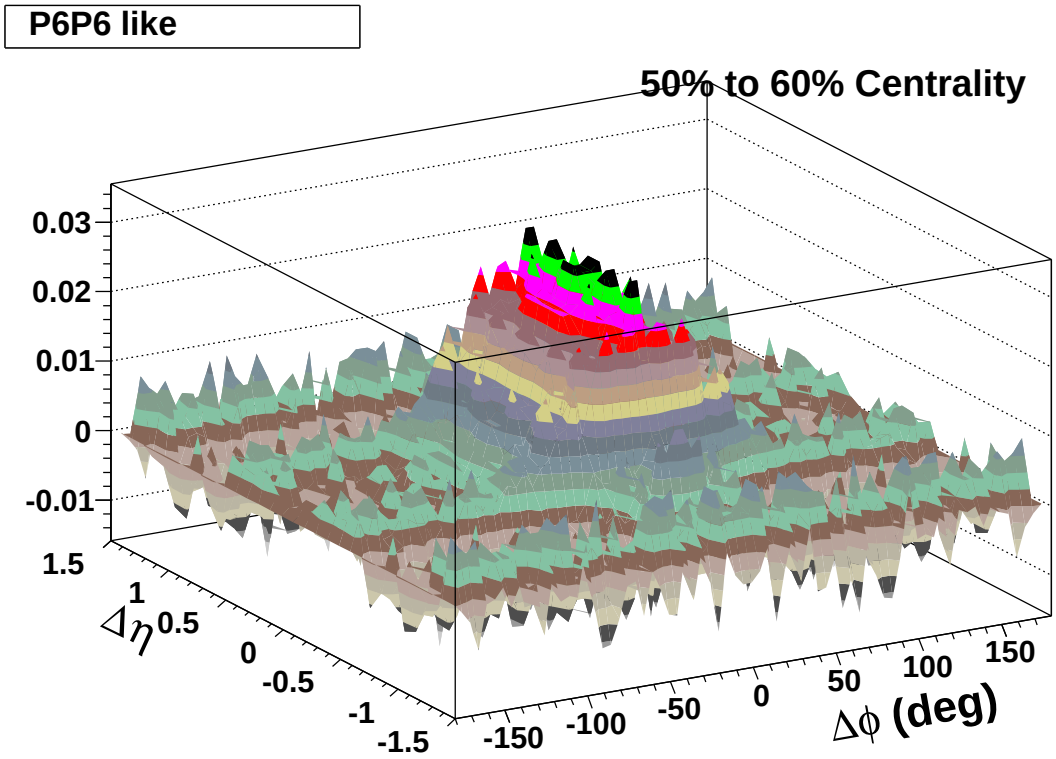


Figure 18: 2-D perspective plot using our extrapolation model(see text) of the like signal for P6P6 $p_t$ cuts(also see text) in the 50%-60% centrality bin.

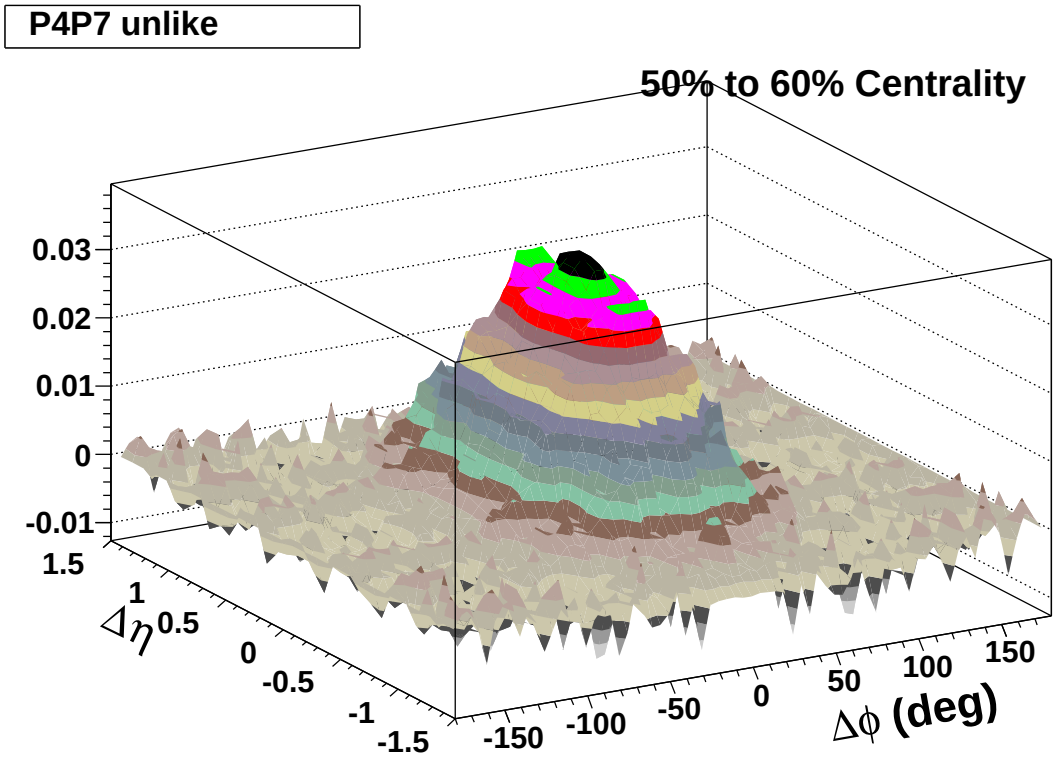


Figure 19: 2-D perspective plot using our extrapolation model(see text) of the unlike signal for P4P7 $p_t$ cuts(also see text) in the 50%-60% centrality bin.

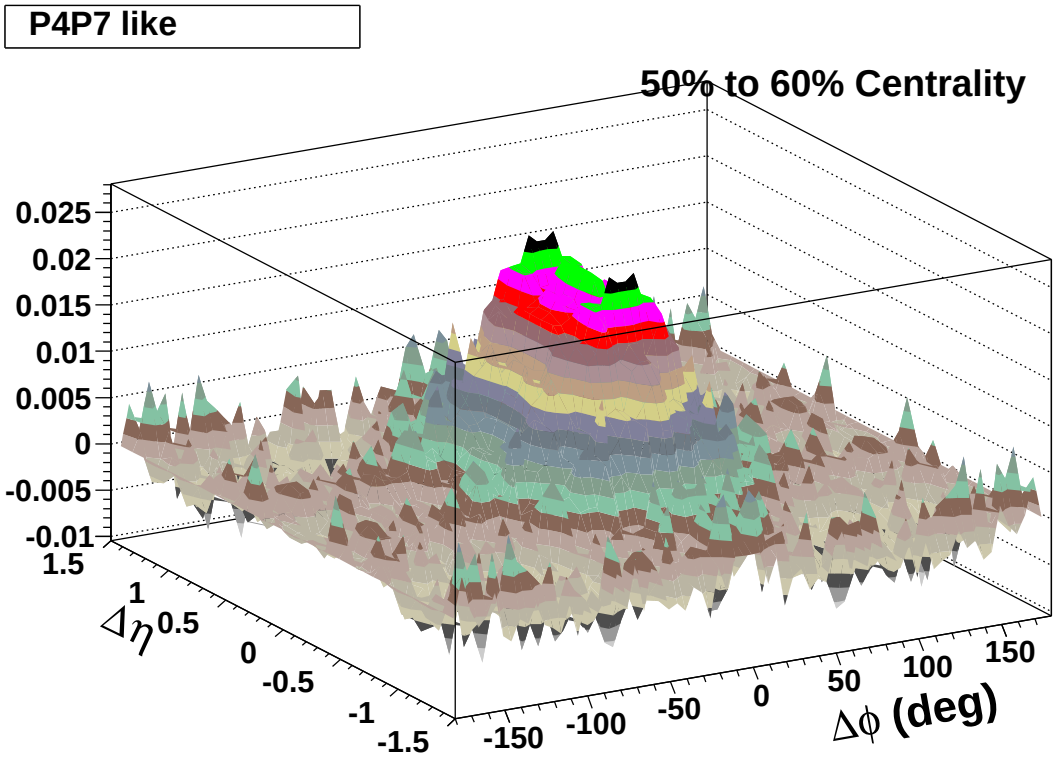


Figure 20: 2-D perspective plot using our extrapolation model(see text) of the like signal for P4P7 $p_t$ cuts(also see text) in the 50%-60% centrality bin.

Therefore if we look at a wider $p_t$ range we should initially see the growth of flux tubes from the surface and the volume with centrality until the point that the volume set start to be destroyed and the surface set is only present. Figure 21 from Ref.[7] shows clearly this effect in the yield of gaussian peak amplitude which show a rapid growth staring at 55% to 65% and continue growing at a rapid rate until 19% to 28% at which the growth slows and turns over. Since many of the particles used in our extrapolation could come from partons that fragment inside the volume we could use Figure 21 to obtain another extrapolation for the whole volume. Our surface extrapolation used Figure 4 with $p_t$ range (0.8 GeV/c $< p_t <$ 4.0 GeV/c) which is a simple linear extrapolation. Figure 22 through Figure 25 show our new volume extrapolation for P6P6 and P4P7 which is about a factor two larger because the peak value remains approximately constant until ∼24% centrality. After this value we used a linear drop off.

We also compare this new dipion effective mass spectrum generated by PYTHIA fragmentation from partons that fragment from the whole fireball. This comparison is also shown in Figure 26 for dipion $p_t$ (1.6 GeV/c $< p_t <$ 1.8 GeV/c). For the spectrum we see that PYTHIA is just an approximation of the true under lying physics. However this comparison does give us hope that the background minijet tail we used in our model fits is of the right level and the right shape for the higher mass dipion effective mass spectrum. Also the level of resonances like the $\omega$, the $\rho(770)$ and $K_S^0$ are mainly generated by minijet fragmentation.

# 4 Summary and Discussion

In this article we start with an altered equation 6 of Part 1. This equation 6 has two components in each orbital state: one being the thermal production of resonances in a dipion orbital state, the other is the re-scattering of dipions coming from parton or minijet fragmentation into the dipion orbital state which do not come directly from the resonance. Unitarity requires that there most be re-scatter through the resonance of the phase shift.

Equation 6 considers only elastic scattering of the $\pi\pi$ system. We considered the Dwave which couples to the $f_2(1270)$ ($J^{PC} = 2^{++}$) with 85% of the cross section in the $\pi\pi$ channel. The Pwave which coupled to the $\rho(770)$ ($J^{PC} = 1^{--}$) where 100% is in the $\pi\pi$ channel. The Swave $\pi\pi$ ($J^{PC} = 0^{++}$) couples to two resonances the $\sigma$ and the $f_0(980)$. The $\sigma$ is purely elastic while the $f_0(980)$ is split between the $\pi\ \pi$ and $K\ \overline{K}$ channels. We saw in Part 1 Sec.3 that the $f_0$ was a narrow resonance. The $f_0$ resonates at the $K\ \overline{K}$ threshold. Direct production of the $f_0$ gives a bump at the $K\ \overline{K}$ threshold and the re-scattering of $\pi\pi$ also gives much the same bump at the $K\ \overline{K}$ threshold (See Sec. 3 of Part 1 Figure 2). Therefore we considered the $f_0$ as a resonance being directly produced and decaying into $\pi\pi$ near the $K\ \overline{K}$ threshold.

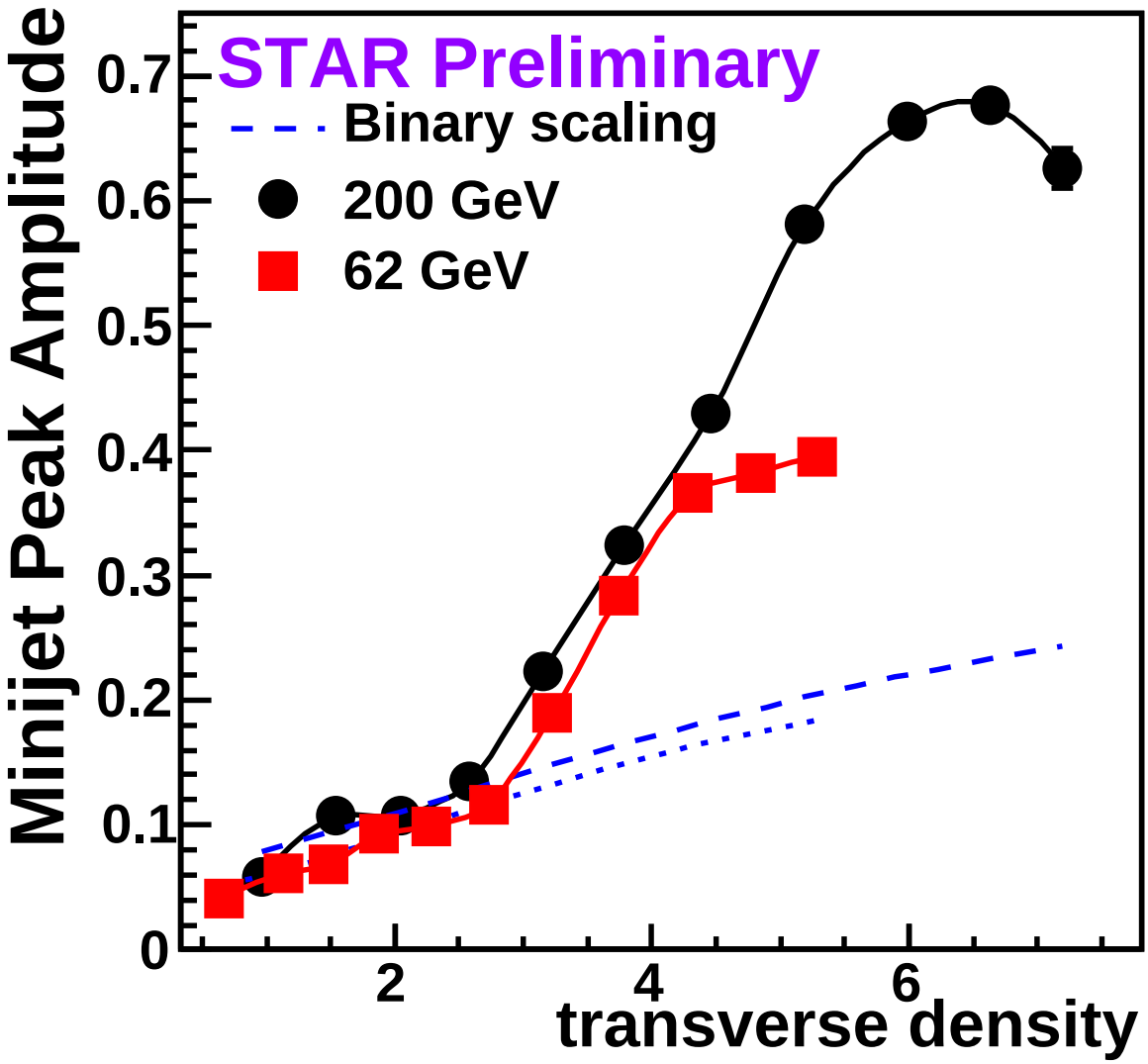


Figure 21: Same-side gaussian peak amplitude fits for Au-Au Collisions at $\sqrt{s_{NN}}$ equal 200 GeV and 62 GeV. Points show eleven centrality bins for each energy (84-93%, 74-84%, 65-74%, 55-65%, 46-55%, 37-46%, 28-37%, 19-28%, 9-19%, 5-9%, and 0-5%) transformed to transverse density.

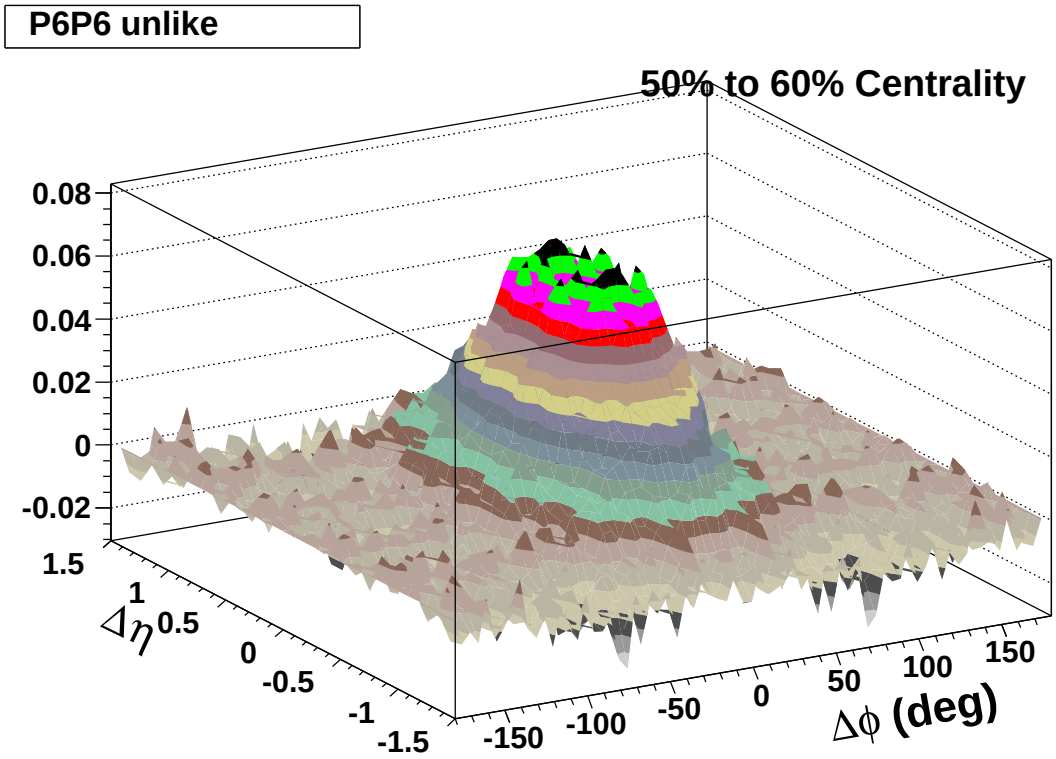


Figure 22: 2-D perspective plot using our extrapolation model for the minijet volume(see text) of the unlike signal for P6P6 $p_t$ cuts(also see text) in the 50%-60% centrality bin.

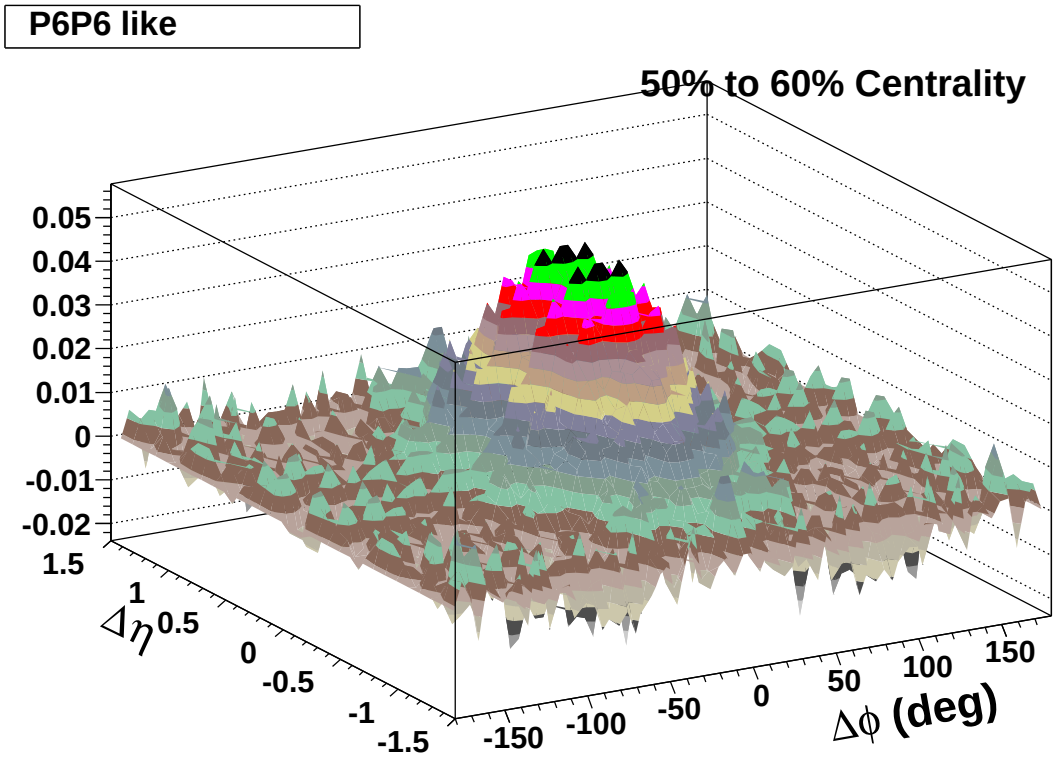


Figure 23: 2-D perspective plot using our extrapolation model for the minijet volume(see text) of the like signal for P6P6 $p_t$ cuts(also see text) in the 50%-60% centrality bin.

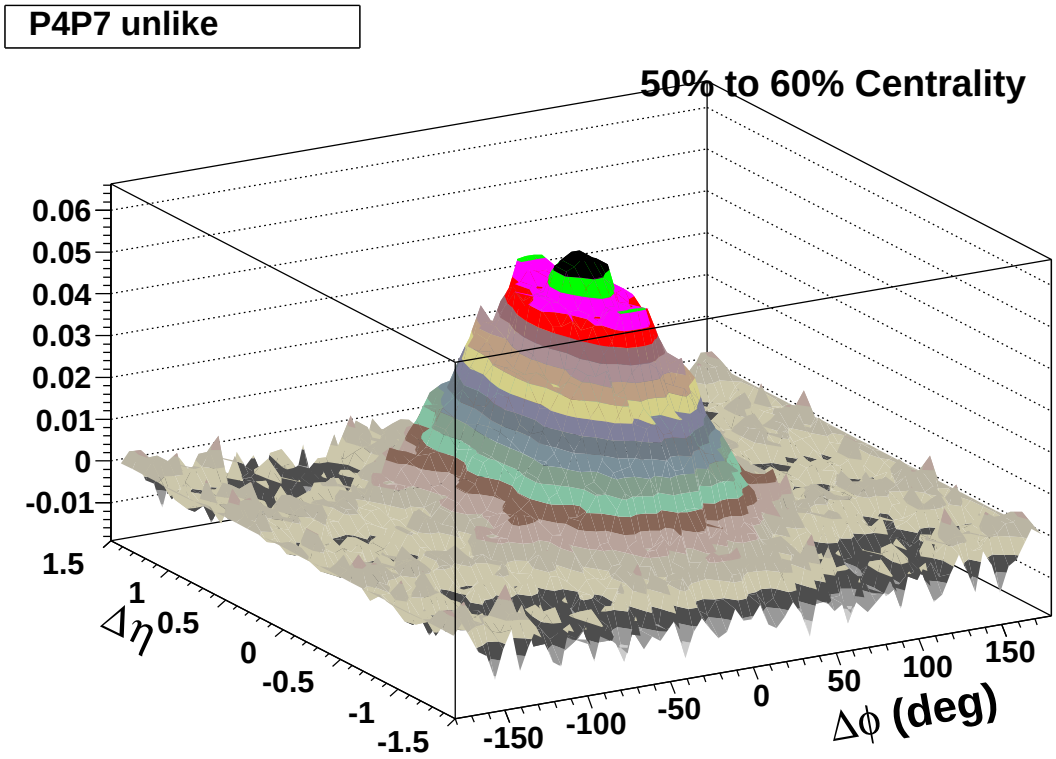


Figure 24: 2-D perspective plot using our extrapolation model for the minijet volume(see text) of the unlike signal for P4P7 $p_t$ cuts(also see text) in the 50%-60% centrality bin.

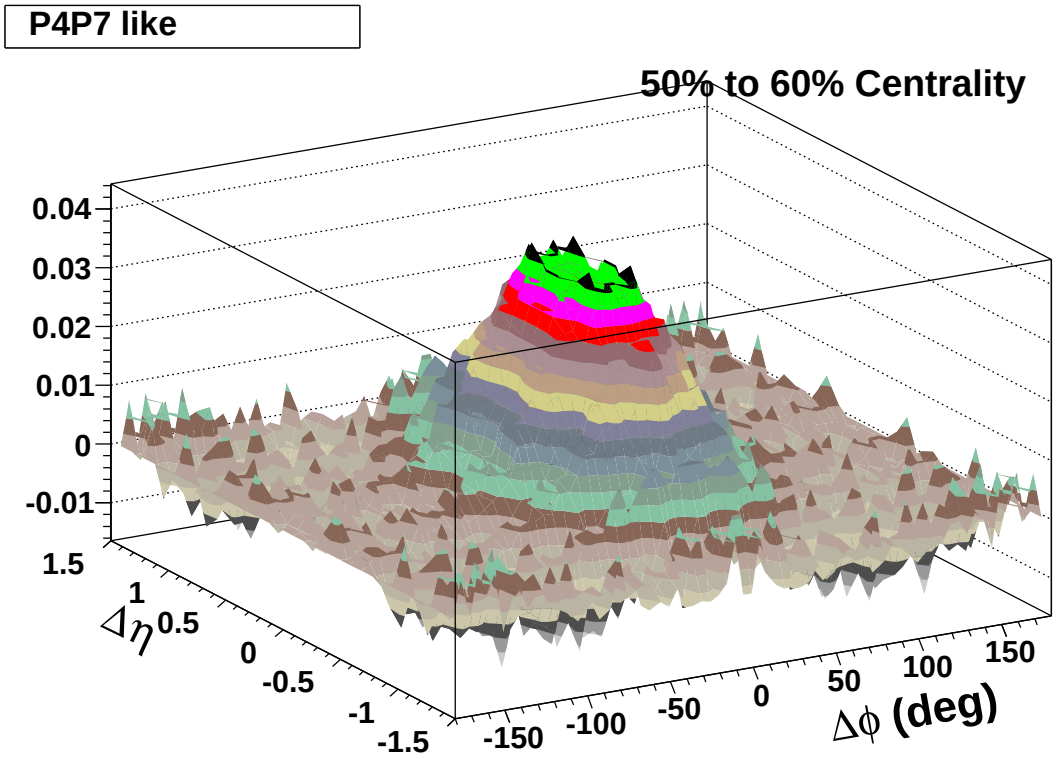


Figure 25: 2-D perspective plot using our extrapolation model for the minijet volume(see text) of the like signal for P4P7 $p_t$ cuts(also see text) in the 50%-60% centrality bin.

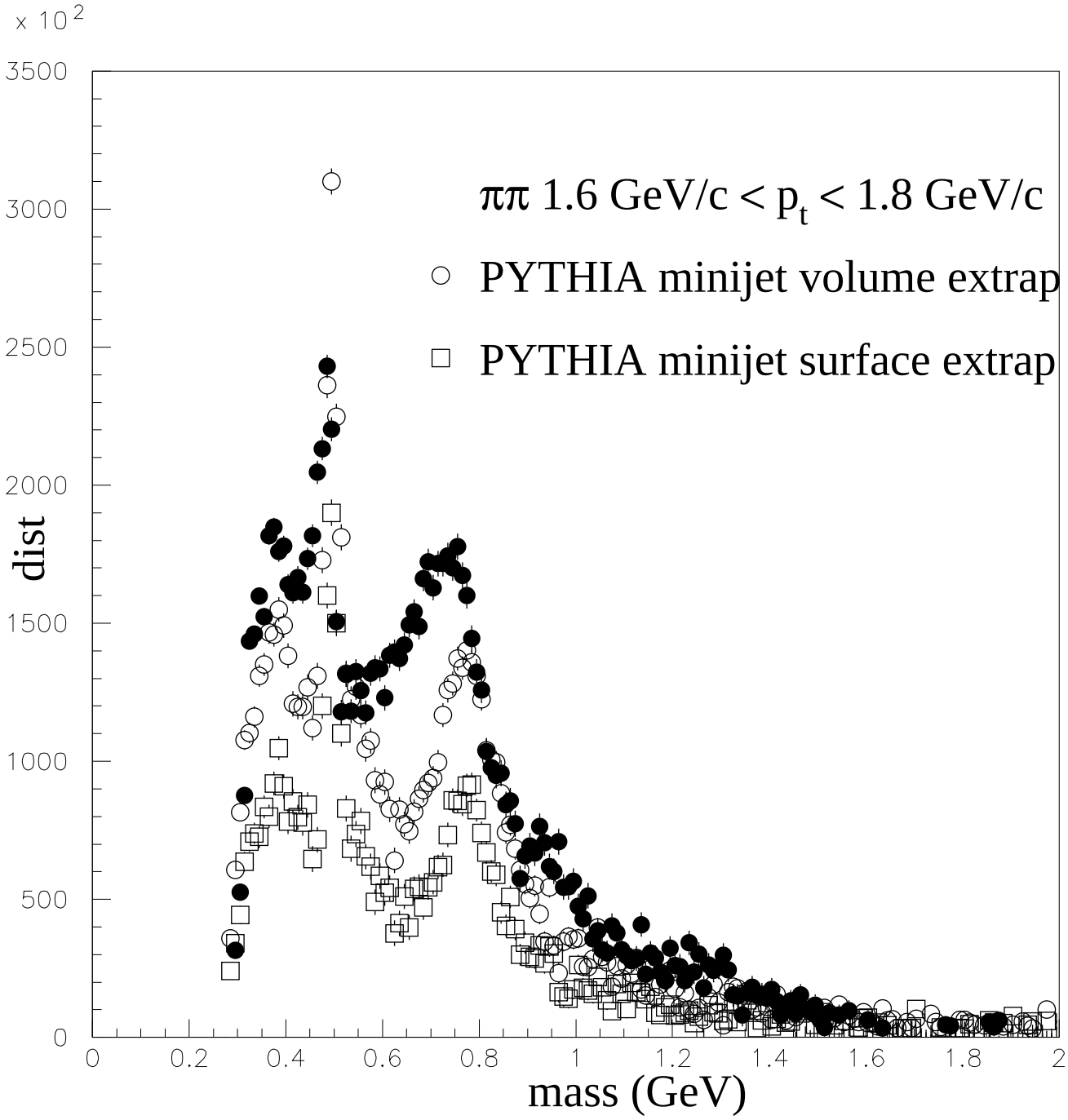


Figure 26: The dipion $p_t$ range 1.6 GeV/c $< p_t <$ 1.8 GeV/c showing STAR data for Au-Au collisions at $\sqrt{s_{NN}} = 200$ GeV. The squares are the surface extrapolation of PYTHIA fragmentation model(see text), while the circles are the volume extrapolation of PYTHIA(also see text).

We chose a dipion $p_t$ range to do a cocktail fit to the effective dipion mass spectrum. We needed three important ingredients in order to do these fits. First is the thermal production of resonances that decay into $\pi^+\pi^-$ as a function of dipion $p_t$. Second is the dipion effective mass spectrum as a function of dipion $p_t$ coming from minijet production not through resonance decay. Third we needed to rewrite equation 6 in a form that uses resonance or Breit-Wigner parameters (mass, widths) instead of phase shifts. Once these three ingredients were developed we were successful in doing a cocktail fit (Figure 1).

A direct measurement of minijets is done through two particle angular correlations[4]. There are two models which can reproduce the angular correlations seen in central Au-Au collisions at $\sqrt{s_{NN}} = 200$ GeV. We use both models for scaling the level of angular correlations expected for our dipion $p_t$ range (1.6 GeV/c $< p_t <$ 1.8 GeV/c) for our centrality. We create a simple model using PYTHIA and HIJING that is a good approximation to the angular correlations. One model (flux tube model) predicts the dipion effective mass spectrum coming from fragmenting partons escaping from the surface of the fireball. This gives a lower limit for the spectrum. The other model (minijet model) considers partons coming from the total volume and gives an upper limit to the spectrum. For these spectrum we see that PYTHIA is just an approximation of the true under lying physics. However this comparison does give us hope that the background minijet tail we used in our model fits are of the right level and the right shape for the higher mass dipion effective mass spectrum. Also the level of resonances like the $\omega$, the $\rho(770)$ and $K_S^0$ are mainly generated by minijet fragmentation.

# 5 Acknowledgments

This research was supported by the U.S. Department of Energy under Contract No. DE-AC02-98CH10886. The author thanks William Love for the STAR analysis of the angular correlation data from Run 4. Also for his assistance in the production of figures. It is sad that he is gone.

# References

[1] T. Trainor, Phys. Rev. C 80 (2009) 044901.

[2] F. von Hippel and C. Quigg, Phys. Rev. 5 (1972) 624.

[3] T. Sjostrand, M. van Zijil, Phys. Rev. D 36 (1987) 2019.

[4] R.S. Longacre, arXiv:1105.5321[nucl-th].

[5] B.I. Abelev *et al.*, arXiv:0806.0513[nucl-ex].

[6] S.J. Lindenbaum and R.S. Longacre, Phys. Rev. C 78 (2008) 054904.

[7] M. Daugherity *et al.*, J.Phys.G G35 (2008) 104090.

[8] X.N. Wang and M. Gyulassy, Phys. Rev. D 44 (1991) 3501.

[9] L. McLerran and R. Venugopalan, Phys. Rev. D 49 (1994) 2233; Phys. Rev. D 49 (1994) 3352; Phys. Rev. D 50 (1994) 2225.

[10] D. Kharzeev, A. Krasnitz and R. Venugopalan, Phys. Lett. B 545 (2002) 298.

[11] T. Lappi and L. McLerran, Nucl. Phys. A 772 (2006) 200.

[12] P. Romatschke and R. Venugopalan, Phys. Rev. D 74 (2006) 045011.

[13] S. Gavin, L. McLerran and G. Moschelli, Phys. Rev. C 79 (2009) 051902.

[14] S.J. Lindenbaum, R.S. Longacre, arXiv:0809.2286[Nucl-th].